3
Micromechanical models of mechanical response of HPFRCC

V.C. LI
University of Michigan, Ann Arbor, MI, USA
H. MIHASHI
Tohoku University, Sendai, Japan
H.C. WU
University of Michigan, Ann Arbor, MI, USA
J. ALWAN
University of Michigan, Ann Arbor, MI, USA
R. BRINCKER
Aalborg University, Aalborg, Denmark
H. HORII
University of Tokyo, Tokyo, Japan
C. LEUNG
Massachusetts Institute of Technology, Cambridge, MA, USA
M. MAALEJ
University of Michigan, Ann Arbor, MI, USA
H. STANG
Technical University of Denmark, Lyngby, Denmark

Abstract
The state-of-the-art in micromechanical modeling of the mechanical response of HPFRCC is reviewed. Much advances in modeling has been made over the last decade to the point that certain properties of composites can be carefully designed using the models as analytic tools. As a result, a new generation of FRC with high performance and economical viability, is in sight. However, utilization of micromechanical models for a more comprehensive set of important HPFRCC properties awaits further investigations into fundamental mechanisms governing composite properties, as well as integrative efforts across responses to different load types. Further, micromechanical models for HPFRCC behavior under complex loading histories, including those in fracture, fatigue and multiaxial loading are urgently needed in order to optimize HPFRCC microstructures and enable predictions of such material in structures under realistic loading conditions.

Keywords: composites, fiber, design, micromechanics, model, high performance.

High Performance Fiber Reinforced Cement Composites 2. Edited by A.E. Naaman and H.W. Reinhardt.
Published in 1996 by E & FN Spon, 2-6 Boundary Row, London SE1 8HN, UK. ISBN 0 419 21180 2.

Contents

1 INTRODUCTION

This chapter reviews the latest advances in micromechanical modeling of high performance fiber reinforced cementitious composites (HPFRCC). It pertains to models of material mechanical response on the composite level. Some work on models on the structural level can be found in Chapters 4, 7 and 8. Investigations of models on the fiber/matrix interface level can be found in Chapter 5.

Micromechanical models described in this chapter attempt to relate microstructural parameters to composite properties. For HPFRCC, microstructural parameters are generally associated with fiber, matrix, fiber/matrix interface, and flaw size. The most important utilities of micromechanical models are: (a) provide physical insight into how composite properties are controlled by material microstructures, and (b) provide guidelines for optimal design of composites. The current state-of-the-art of most micromechanical models are far from these ideals, but are clearly making progress continuously. Micromechanical models are expected to play an increasingly important role in systematic engineering of HPFRCC, reducing the amount of empiricism in materials engineering, and making possible targets of microstructure tailoring for composite property optimization. As a result, micromechanical models can make the difference between an ordinary FRC and a HPFRCC. It is expected that micromechanical models will provide the driving force for critical selection of mineral admixtures, aggregate selection, and fiber design in truly high performance FRCC.

The basic ingredients of micromechanical models include: 1) isolating the important micromechanism(s) responsible for a particular composite response, and 2) isolating the important microstructures associated with these micromechanisms. A good micromechanical model should include just enough details of micromechanisms and microstructural parameters to describe the composite behavior, but not too much to overwhelm the analyses with 'noise'. The most useful models are characterized by parameters which are physically measurable (although not always 'easy' to measure). This is particularly important if the models are used for composite microstructure tailoring.

This chapter is organized according to models of the most important mechanical properties, including tension, compression, flexure, fracture toughness, and elastic stiffness. The discussion and concluding section provides a combined overview of these various sections and properties, evaluates the current state of affairs in micromechanical model development, and projects the most urgently needed micromechanics research in HPFRCC.

2 UNIAXIAL TENSILE RESPONSE

2.1 Introduction

When unreinforced cementitious materials fail under tension, the brittle failure is accompanied by the formation of a single crack (Fig.1a). For fiber reinforced cementitious composites, depending on the effectiveness of fibers in providing crack bridging stresses, different failure modes can be resulted [1,2]. If the fibers cannot carry further load after the formation of the first through crack, the first cracking strength is the ultimate strength and further deformation is accompanied by material softening with the opening of a single crack (Fig.1b). If the fibers can support further loading after first cracking, multiple cracking occurs (Fig.1c). The stress-strain behavior then exhibit pseudo strain hardening (Fig.2) before the ultimate strength is reached at a very high strain (up to 8% in Fig.2, tens to hundreds of times the strain capacity of the unreinforced matrix material). This is a fundamental material characteristic of HPFRCC.

In order to achieve the desirable pseudo-strain hardening behavior, two criteria have to be satisfied: (i) steady state cracking criterion, that is, a crack can propagate at a constant (or steady state) stress as the fiber bridging stress in the middle of the crack becomes equal to the applied tensile stress, and (ii) the further cracking criterion, which requires the inherent crack size to be large enough for the first cracking stress to be

lower than the maximum bridging stress. Additional cracks can then form on further loading.

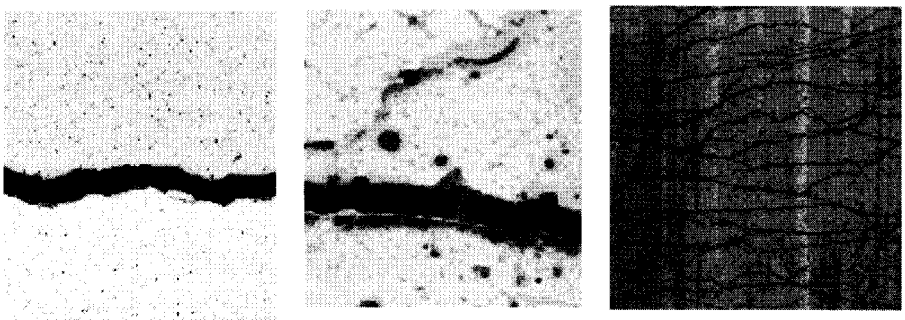

(a) (b) (c)

Figure 1. Computer Scanned Images of (a) Plain Cement Showing Brittle Failure, (b) FRC Showing Single Crack Opening and (c) ECC Showing Multiple Cracking [3].

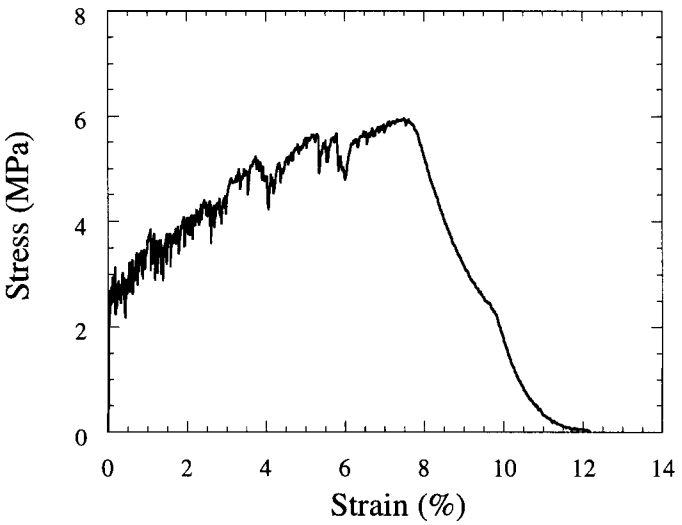

Figure 2. Tensile Stress-Strain Curve of Polyethylene Fiber Reinforced Cement Paste (V_f=2%) [4].

2.2 Behavior before First Cracking

Before the first through crack is formed, the tensile stress strain curve is usually very linear. However, with the use of optical microscopy and laser holographic interferometry, Stang et al [5] and Mobasher et al [6] show that the propagation of microcracks starts at stress levels well below the first cracking strength. Theoretical analysis of microcrack propagation and interface debonding processes before first

cracking has been carried out by Yang et al [7]. By modelling both cracks and fibers as inclusions in an elastic body, several possible damage development stages before first cracking can be identified. The analysis shows that if the fiber volume fraction is higher than a critical value, fiber debonding will not occur before first cracking. While the first cracking strength increases with increasing fiber volume fraction, the energy absorption up to the occurrence of first cracking reaches a maximum.

2.3 The Steady State Cracking Criterion

In HPFRCC, the Griffith type crack in brittle material is replaced by flat steady state crack [1]. This mode of cracking is necessary for pseudo strain-hardening in HPFRCC. In the following, the criterion for steady state cracking to occur are derived based on an energy balance argument [2].

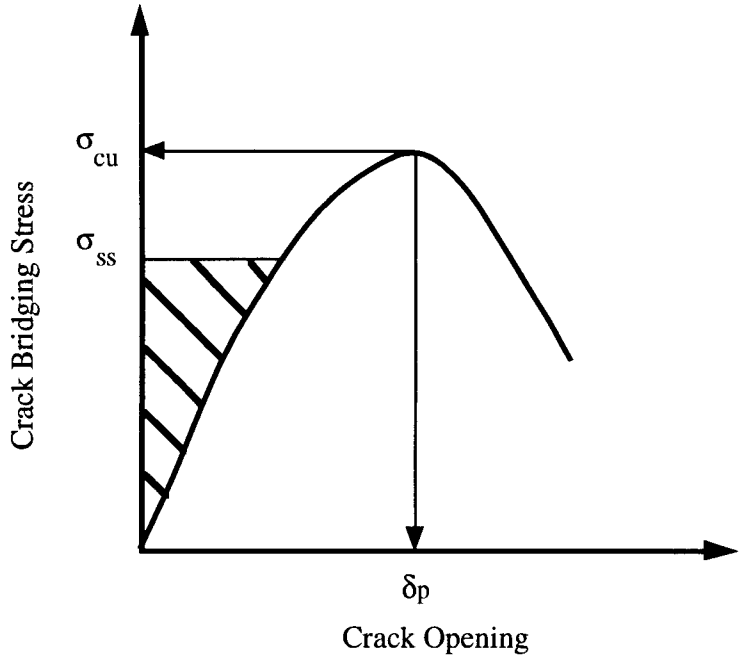

Figure 3. A Typical σ-δ Relation for Fiber Composites [2].

Fig.3 shows the σ-δ relation for an arbitrary fiber composite. σ_{cu} is the maximum bridging stress while δ_p is the crack opening at which the maximum crack bridging stress is reached. Fig.4 shows a through crack lying along the x-axis under uniaxial tensile stress in the y-direction. For the crack to extend by an amount Δa on each side (Fig.4b), the additional work done on the system (dW) must be equal to the sum of the strain energy change of the system (dU) and the energy for forming the new crack surface (dE_S). If steady state cracking occurs, the applied stress remains constant at σ_{ss} as a small crack increases in size to form a through crack with part of the crack profile remaining flat at a constant crack opening δ_{ss} [1, 8, 9]. By definition, σ_{ss} is the first cracking strength. Then, by comparing Fig.4a and 4b for the configurations

before and after crack extension, it is obvious that the strain energy change dU of the system is equal to two times the energy difference between a strip of material Δa in length perpendicular to the flat part of the crack profile (A-A in Fig.4b) and a strip of the same size in the un-cracked material far away from the crack tip (B-B in Fig.4b). The additional work done on the system is due to a displacement δ_{ss} of the applied stress over the newly formed crack surface of length $2\Delta a$. The change in surface energy is equal to G_{tip} (the crack tip critical energy release rate of the composite) times the newly formed crack area. For a unit thickness of the specimen:

$$dW = (2\,\Delta a)\,\sigma_{ss}\,\delta_{ss} \tag{1}$$

$$dU = (2\,\Delta a)\left[\int_0^{\delta_{ss}} \sigma(\delta)d\delta\right] \tag{2}$$

$$dE_s = (2\,\Delta a)\,G_{tip} \tag{3}$$

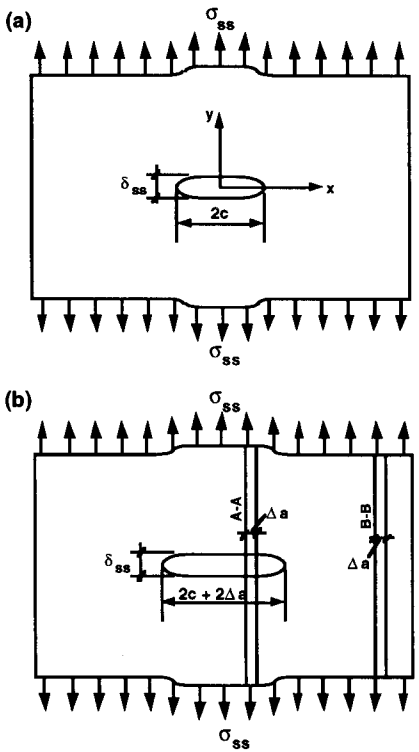

Figure 4. Crack Extension under Steady State Condition [2].

The condition of energy balance, $dW = dU + dE_s$ gives:

$$\sigma_{ss}\,\delta_{ss} - \int_0^{\delta_{ss}} \sigma(\delta)d\delta = G_{tip} \tag{4}$$

The left hand side of eqn(4) represents the complementary energy of the σ-δ curve shown by the shaded area in Fig.3. If the σ-δ relation for a given composite is known, the first cracking stress σ_{ss} can be readily obtained. For steady state cracking to be possible, the complementary energy has to reach the energy for crack propagation, G_{tip}. Since the complementary energy reaches its maximum value when σ_{ss} equals σ_{cu} (see Fig.3), the condition that makes steady state cracking possible is given by:

$$\sigma_{cu}\,\delta_p - \int_0^{\delta_p} \sigma(\delta)d\delta \geq G_{tip} \tag{5}$$

Eqn(4) and eqn(5) are first derived respectively by Marshall and Cox [10] and Li [11]. Since the analyses in Marshall & Cox and Li are based on the J integral, the crack tip fracture resistance term is denoted by J_{tip} rather than G_{tip}. Eqns (4) and (5) are generalized equations, and their applications to various fiber composite systems with known σ-δ relations can be found in Marshall and Cox [10], Li [11] and Leung [2].

The σ–δ relation in FRC can be written in general form:

$$\sigma = \sigma(\delta; \text{fiber, interface, and matrix characteristics}) \tag{6}$$

A simple form of eqn (6) is available [12] based on micromechanical model of the bridging mechanism of randomly oriented short straight and flexible fibers:

$$\sigma(\delta) = \begin{cases} \sigma_{cu}\left[2\left(\delta/\delta_p\right)^{1/2} - \left(\delta/\delta_p\right)\right] & \text{for } \delta \leq \delta_p \\ \sigma_{cu}\left(1 - 2\delta/L_f\right)^2 & \text{for } \delta_p \leq \delta \leq L_f/2 \\ 0 & \text{for } L_f/2 \leq \delta \end{cases} \tag{7}$$

where $\delta_p = \tau L_f^2/[E_f d_f (1+\eta)]$ is the crack opening corresponding to the maximum bridging stress (Fig.3).

$$\sigma_{cu} = \frac{1}{2} g \tau V_f \frac{L_f}{d_f} \tag{8}$$

In Eqs. (7), V_f, L_f, d_f, and E_f are the fiber volume fraction, length, diameter and Young's Modulus, respectively. τ is the fiber/matrix frictional bond strength. The

snubbing factor $g = 2\left(1+e^{f\pi/2}\right)/\left(4+f^2\right)$ raises the bridging stress of fibers bridging at an angle inclined to the matrix crack plane, appropriate for flexible fibers exiting the matrix analogous to a rope passing over a friction pulley. The snubbing coefficient f must be determined experimentally for a given fiber/matrix system [13]. Finally, $\eta = (V_f E_f)/(V_m E_m)$, where V_m and E_m are the matrix volume fraction and Young's Modulus, respectively.

More sophisticated σ-δ relation which accounts for fiber rupture can be found in [14]. The effect of fiber length variation on the σ-δ relation is discussed in [15].

Based on eqn (7), the critical fiber volume fraction was shown to be [11]:

$$V_f \geq V_f^{crit} \equiv \frac{12 J_{tip}}{g\tau(L_f / d_f)\delta_p} \tag{9}$$

Eqn (9) expresses the condition for steady state cracking necessary for pseudo strain-hardening in the form of a critical fiber volume fraction which must be exceeded to create a composite with high strain capacity. Such condition has been successfully used in the design of pseudo strain-hardening mortars [16]. In Fig. 5, the matrix toughness is plotted against the interface bond strength for a fixed critical fiber volume fraction of 2%, based on Eqn (9). This curve demarcates the boundary between strain-hardening and quasi-brittle failure modes for composites with V_f=2%. All combination of (τ, J_{tip}) to the left of this curve correspond to composites expected to show quasi-brittle behavior. On the other hand, all combinations of (τ, J_{tip}) to the right of the curve correspond to composites expected to show pseudo strain-hardening. It has been confirmed from uniaxial tensile tests that Mix I, IIIa, and IIIb, which (τ, J_{tip}) values lie to the right of the theoretical boundary line, do show pseudo strain-hardening, whereas Mix II does not, as predicted by the theory [16]. The different composites have different values of J_{tip} and τ controlled by matrix mix design via sand content and w/c ratio. Partial verification of the multiple cracking condition was also reported by Krenchel [17] with matrix and interface properties modified by clay addition. Although some of the microparameters (such as snubbing factor and interface bond strength) were estimated, reasonable agreement between predictions and experimental results was found.

In using (9) to calculate V_f^{crit}, it should be pointed out that the crack tip fracture energy J_{tip}, interpretable as the energy consumed per unit advance of the matrix crack (by breaking the matrix material (but not the fiber) at the crack tip region), can only be treated (approximately) as a constant when the fiber volume fraction is small. Otherwise the full form of J_{tip} involving the $(1-V_f)$ term given in (1.16) should be used. Obviously, the only meaningful solution for V_f^{crit} is between 0 and 1. For some combinations of micromechanical parameters such as small fiber aspect ratio L_f/d_f or bond property τ, eqn. (9) will not give any meaningful solution. This should be expected since for such micromechanical parameters, the energy condition for steady state cracking condition expressed in (5) cannot be satisfied. This means that pseudo strain-hardening cannot occur when the fiber is too short or when the interfacial bond strength is too low. In such circumstances, composites with even a large amount of

fiber (hypothetically approaching 100%) should still not be expected to undergo strain-hardening.

2.4 Condition for Further Cracking

In order for additional cracks to form after first cracking, the first cracking strength σ_{fc} should be lower than the peak bridging stress σ_{cu}. This condition is supplementary to eqn (9) for multiple cracking [1]. In general, the first cracking strength for a given inherent crack size can only be computed after the exact crack profile is obtained through an iterative procedure. An approximate value of σ_{fc} can be obtained, however, by assuming a parabolic crack profile.

$$\delta(x) = 4(1-\nu^2)K_{tip}c^{1/2}(1-x^2/c^2)/(E_c\pi^{1/2}) \tag{10}$$

Let $c=c_{mc}$ when $\sigma_{fc}=\sigma_{cu}$. Since σ_{fc} decreases with c, the condition for further cracking ($\sigma_{fc}<\sigma_{cu}$) can be given in terms of crack size as:

$$c>c_{mc} \tag{11}$$

with c_{mc} given by the solution of the following equation:

$$\sigma_{cu}(\pi c_{mc})^{1/2} - 2(c_{mc}/\pi)^{1/2}\int_0^{c_{mc}} \sigma[\delta(x)]/\left(c_{mc}^2 - x^2\right)^{1/2} dx = K_c \tag{12}$$

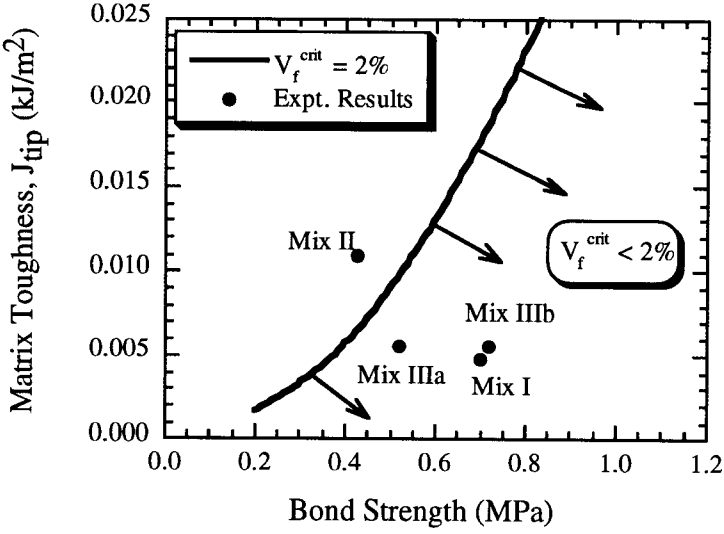

Figure 5. Effect of Matrix Fracture Toughness and Interface Bond Strength on Critical Fiber Volume Fraction (E_f=117 GPa, L_f=12.7 mm, d_f=0.038 mm, g=2, E_m=25 GPa) [16].

Once the composite σ-δ relation is known, the substitution of (10) into (12) would allow c_{mc} to be determined. With the approximate profile, the first cracking strength vs crack size curve is shifted upwards, giving an apparent c_{mc} higher than the actual value (Fig.6). By overestimating c_{mc}, the approximate analysis provides a conservative criterion for further cracking to occur. Since it is very difficult to precisely measure the inherent crack size in the composite, the use of an approximate but conservative criterion is actually advantageous.

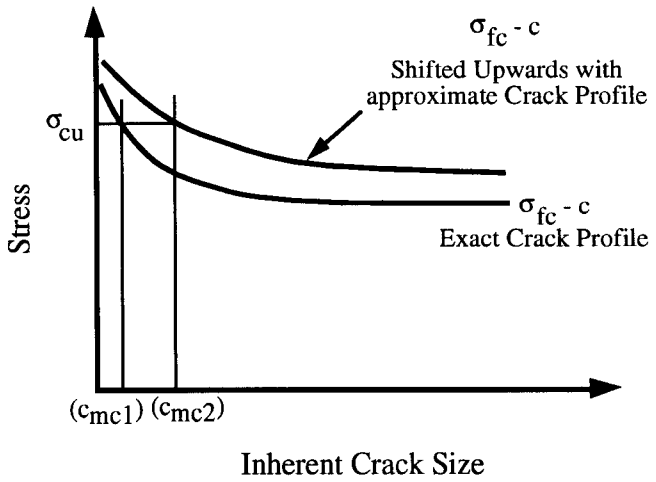

Figure 6. Overestimation of c_{mc} with an Approximate Crack Profile [2].

The pair of equations (9) and (11) together form the complementary conditions for pseudo strain-hardening to occur in random fiber reinforced cementitious composites. If only (9) is satisfied but not (11), the load to initiate the first crack can be much higher than bridging load capacity of the fiber after the matrix crack propagates through the specimen cross-section. This leads to a loss of equilibrium (unless ambient load drops immediately after first crack initiation) and immediate failure of the specimen. No strain-hardening can result. If only (11) is satisfied but not (9), the load to initiate the first crack may be low relative to the maximum bridging stress. However, as the first crack propagates in a (crack-tip modified) Griffith crack mode, the increasing opening of the (modified) ellipsoidal crack faces as the crack length extends will eventually exceed δ_p (Figure 3), resulting in fiber pull-out and softening in the bridging curve. When the first crack completely traverse the whole specimen width (implying results are specimen size dependent), the remaining load carrying capacity of the fibers still bridging the crack can be much lower than the ambient load. Again, an instability will set in and no further multiple crack or pseudo strain-hardening can occur.

2.5 Multiple Cracking Regime

In the original ACK model [18] and several other subsequent models (e.g. [1], [8]), uniform distribution of identical flaw size in the matrix is implicitly assumed. Consequently, a deterministic single-valued composite strength during multiple cracking is predicted resulting in a "yield plateau" in the stress-strain curve, and usually

does not agree with experimental findings. As shown in Fig. 2, a rising load carrying capacity beyond the first cracking strength is often observed during multiple cracking stage. Multiple cracks develop over a wide range of load levels in a sequential manner. Wu and Li [19] have proposed a stochastic treatment of multiple cracking. In their analysis, the flaw size distribution of the matrix is simulated by a Monte Carlo process, and the crack growth criteria is determined by a fracture mechanics approach. The larger cracks propagate at the first cracking strength, whereas the smallest crack can only be activated at the maximum bridging strength which also marks the end of multiple cracking. For those cracks ranging in between the two extremes, propagation takes place during multiple cracking stage. Good agreement between simulation results and experimental data on crack evolution was found, as shown in Fig. 7.

In a somewhat different approach, Alwan [20] discretized the composite into a number of finite composite elements whose stiffnesses and mechanical properties are updated based on the local deformation of each element using a finite element program. This model identifies various stages and key points characterizing a composite stress-strain curve, such as the composite stress and corresponding strain at first cracking, during multiple cracking, at end of multiple cracking and up to failure of the composite. Fiber bridging stresses, both in the elastic debonding and frictional pull-out stages, are incorporated in the stiffness computation of cracked composite elements using a rotating crack model. Further discussion on this computer model is included in Chapter 7.

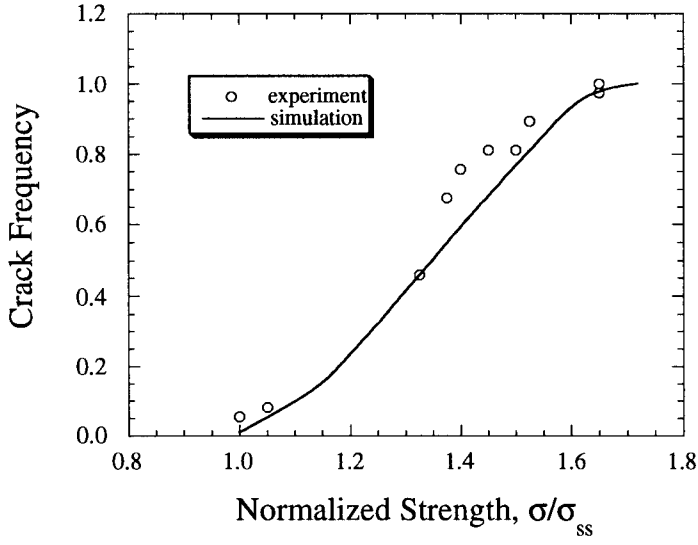

Figure 7. Comparison of Crack Frequency vs Composite Strength (Normalized by the Steady State Strength) between Experimental Data and Simulation Results, m=2 and λ=300 (Both Are Constants Used in the Flaw Size Distribution Function) [19].

2.6 Effect of Interfacial Dual Slip on Multiple Cracking

In the original model of Aveston, Cooper and Kelly who deal with continuous aligned fiber and other models discussed in the above sections, fibers were considered

monolithic and debonding only allowed at the fiber/matrix interface. However, in addition to single fibers (monofilament), fibers are often used in a bundle form (strand) or in the shape of fibrillated film. For such fiber composites, slip occurs both within the strand and at the fiber/cement interface. Ohno and Hannant [21] modeled this phenomenon by permitting dual slip of fibers either inside the bundle (core fiber) or at the interface (sleeve fiber). Figure 8 shows strain distribution near a crack face just after the matrix has cracked. Since strain and stress in the matrix at the crack face become zero, all load is sustained by the fiber. Once the slip between core fibers and sleeve fibers occurs, the core fibers and the sleeve fibers carry different loads and deform according to their individual stress transfer capacity. The characteristic point of this model is that the interface of the sleeve fibers and matrix has the ability to transfer further higher stress after the saturation of multiple cracks under a lower stress transfer within the core fibers. Therefore, a secondary multiple cracking region exists after Point A in Figure 9. Much better agreements between experimental data and theoretical predictions of the tensile stress/strain curves are found when the dual slip phenomenon is considered, especially a reduced V_f is used in the secondary multiple cracking region [21], as shown in Figure 10.

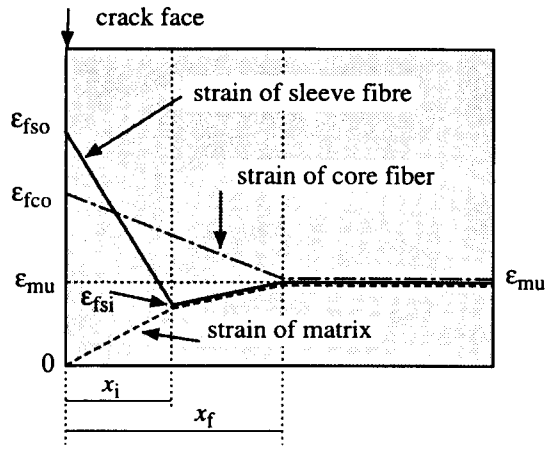

Figure 8. Strain Distribution just after First Cracking [21].

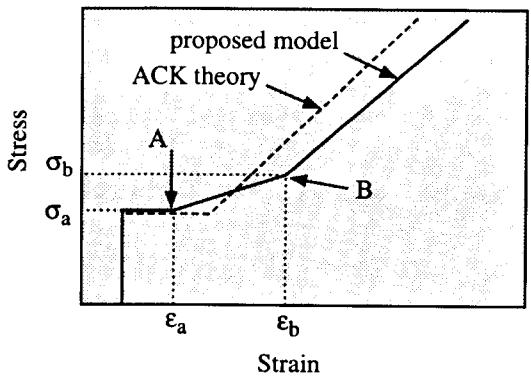

Figure 9. Schematic Diagram of Tensile Stress Strain Curve [21].

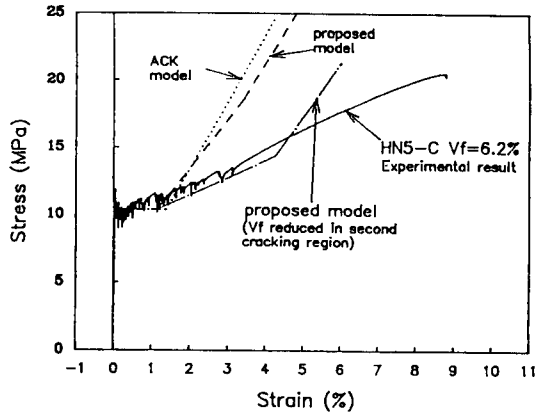

Figure 10. Comparison between Experimental and Predicted Tensile Stress Strain Curves [21].

2.7 Tensile Behavior of HPFRCC with Main Reinforcements

The tensile behavior of HPFRCC with main steel reinforcements has been measured by Al-Shannaq [22] and modelled by Brincker [23]. Some typical tensile response for various volume fractions of main steel and steel reinforcements are shown in Fig.11. Note that for this fiber and matrix system, pseudo-strain hardening cannot be achieved in these composites with the fiber reinforcement alone (Fig.12). That is, the condition given in eqn (9) is not satisfied, probably due to the low fiber aspect ratio despite the high interface bond property [22]. The addition of main reinforcements, however, lead to a pseudo-ductile behavior. The composites containing both main and fiber reinforcements are hence considered HPFRCC in this section.

After first cracking, the matrix stress at the cracked section decreases as the main reinforcement carries more load. By assuming uniform friction along the main reinforcement/matrix interface, and by decoupling the σ from δ in the FRC, the stress to be carried by the matrix at the cracked section was calculated approximately [23] and is shown schematically as a function of crack opening w in Fig.13, for both light reinforcement and heavy reinforcement. The material softening behavior (referred to as the crack opening relation in the figure) is also shown. As long as the stress to be carried is less than the material resistance given by the softening relationship, the crack opening remains controlled. It is clear from the figure that the use of heavy reinforcement can help control the stability of crack opening. For a parabolic softening relation, which is representative of matrix with relatively high steel fiber volume fractions, the stability of cracks can be assessed with a brittleness number B_r, given by:

$$B_r = \frac{1}{6}\frac{E_c(1-\varphi)f_t}{\tau E_r \varphi^2}B_o \qquad (13)$$

with $B_o = \frac{f_t^2 r}{E_m G_f}$ being the traditional brittleness number for homogeneous materials.

In the above expressions, f_t is the matrix strength, E_m is the matrix stiffness, E_c is the composite stiffness, E_r is the reinforcement stiffness, G_f the composite fracture energy, r the radius of the main reinforcement, τ the constant shear stress at the reinforcement/concrete interface and φ the main reinforcement ratio.

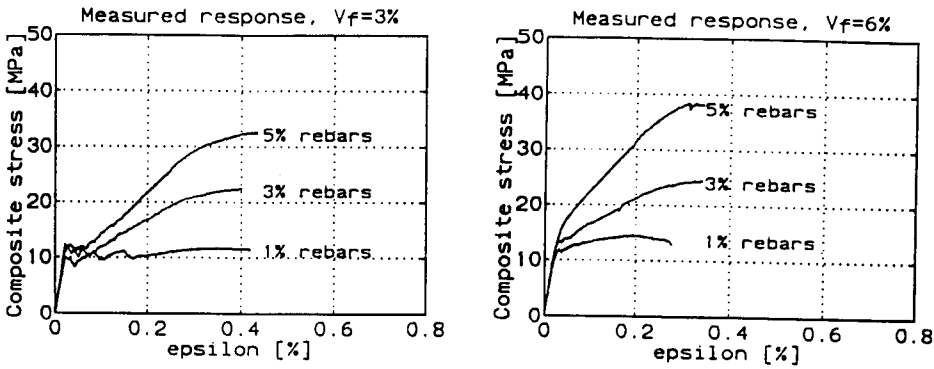

Figure 11. Measured Responses in Uniaxial Tension (a) V_f=3% (b) V_f=6% [23].

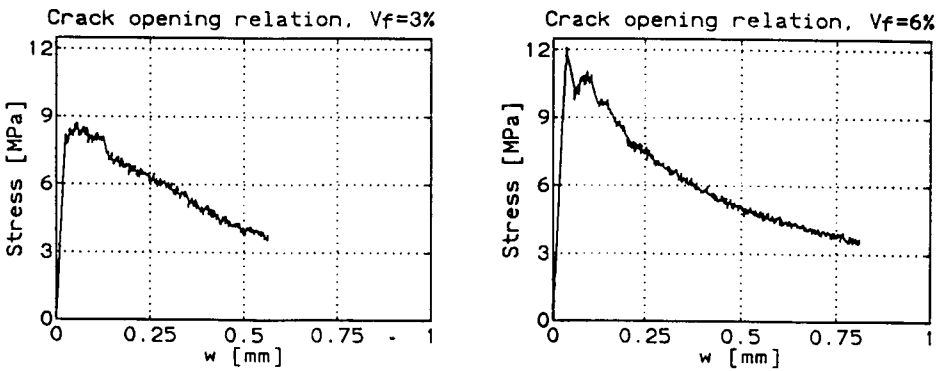

Figure 12. Measured Responses for Notched Specimens without Main Reinforcement (a) V_f=3% (b) V_f=6% [23].

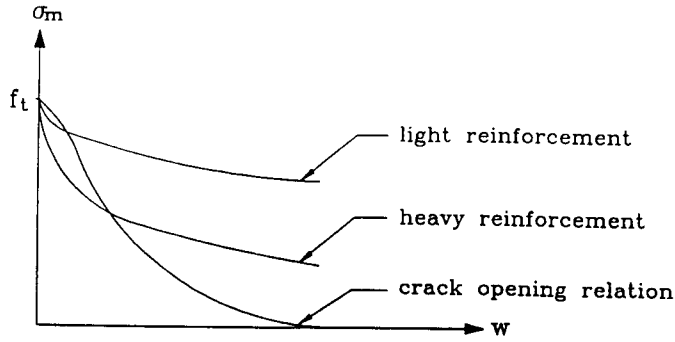

Figure 13. Model Solutions for Light and Strong Main Reinforcement Compared to Material Resistance, the Crack Opening Relation [23].

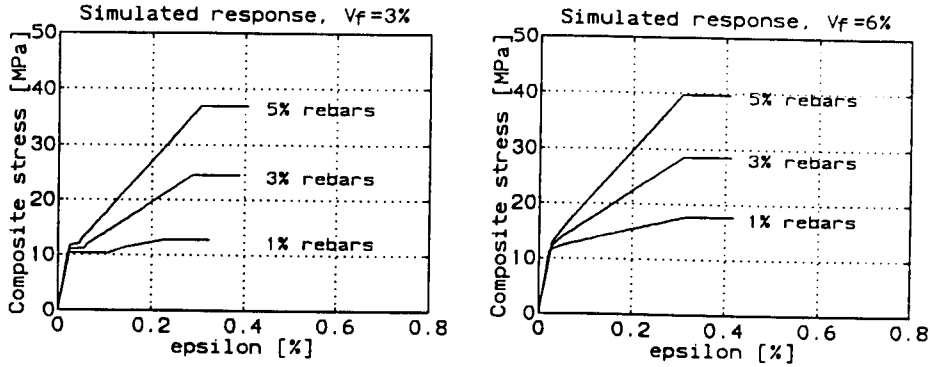

Figure 14. Responses in Uniaxial Tension Simulated by the Presented Model (a) V_f=3% (b) V_f=6% [23].

If B_r is well below one, cracks will grow stably, resulting in a well distributed crack pattern. On the other hand, if B_r is well above one, unstable cracks are expected to form, resulting in larger discrete cracks.

For matrix with low or moderate volume of steel fibers, the load carrying capacity of the fibers alone are lower than that of the reinforced matrix at first cracking. As a result, the softening relation shows a sudden drop Δf_t right after first cracking. Then, the strain of the composite will increase at constant stress by an amount $\Delta\varepsilon$, given by:

$$\Delta\varepsilon = \frac{1-\varphi}{2E_r\varphi}\Delta f_t \qquad (14)$$

A sudden increase in strain at roughly constant stress can be observed in Fig.11 for the case with V_f=3%.

Based on the concepts described above, and assuming elastic steel behavior and plastic matrix behavior, the stress strain relationships for composites with both main and fiber reinforcements are derived and shown (Fig.14). With slight adjustments in model parameters, the derived tensile response shows good qualitative agreement with experimental data (Fig.11).

A more complete solution for tensile response of HPFRCC with both fiber and main reinforcements is given by Stang and Aarre [24]. In their analysis, the main reinforcement is assumed to remain elastic. Shear lag analysis are first carried out to obtain the crack openings for two separate cases: (i) load acting on the main reinforcement, and (ii) load acting only on the matrix, with main reinforcement displacement restrained to be zero at the crack. Solutions of the two separate cases are then superposed to ensure that the σ-δ relation of the fiber reinforced matrix is satisfied at the crack. With this approach, for different fiber reinforced matrices (i.e., different σ-δ relations), the crack width can be obtained as a function of main reinforcement ratio and fiber volume fraction for any given imposed far field strain. When fibers are added, the reduction in amount of main reinforcement for crack opening control can be quantified.

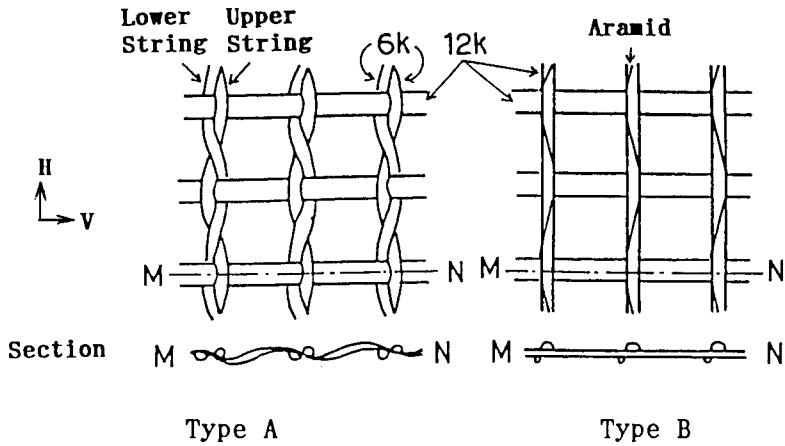

Figure 15. Weaving Structure of Carbon Fiber Mesh [26].

2.8 Effect of Fiber Weaving Structure on Tensile Behavior of HPFRCC

In addition to single filament and fiber bundle, fiber mesh is also being explored to reinforce brittle concrete [25, 26]. Different weaving patterns of carbon fiber mesh, as shown in Figure 15, were used by Mihashi et al [26] to examine reinforcement efficiency in mortar. A significant influence of the weaving structure on the flexural response was discovered. Type A mesh (see Fig 15) exhibited the largest ductility. On the other hand, Type B mesh demonstrated the highest strength but the behavior after the peak load was most brittle. It is expected that similar conclusions may be drawn

when the specimens are tested under direct tensile tests, since the flexural response of fiber reinforced mortar is controlled by its tensile failure. Stress analysis of these mesh reinforcements are described by Mihashi et al, and shown in Figure 16. In the case of Type A mesh arranged in H direction, the splitting stress due to the tortuosity of strings are eliminated by the coupling strings and gradual debonding was controlled by microcracks accumulated along the strings. It may be the reason why Type A mesh gave such a large ductility. In the case of Type B mesh, strings with crossing points might work just like wedges to split the cover mortar. Detailed stress analysis is needed to quantify the effect of mesh weaving structure on the tensile response of HPFRCC, thus providing rationals for composite design.

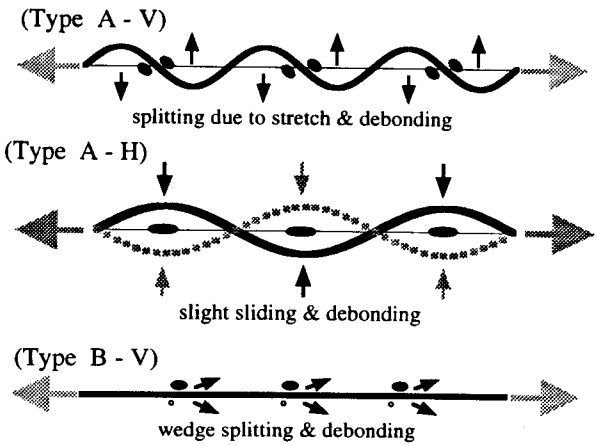

Figure 16. Schematic Description of Stress Analysis of Mesh Reinforcement [26].

2.9 Conclusion

The tensile behavior of HPFRCC is shown to be highly sensitive to micromechanical parameters via the composite σ-δ relation. With appropriate choice of fiber, matrix and interface parameters, it is possible to develop HPFRCC with the proper σ-δ relation such that the brittle cementitious material fundamentally changes into a pseudo strain-hardening composite. Analytic micromechanical models provide explicit conditions and composite design tools for transition from quasi-brittle softening response of typical FRC to significantly more ductile hardening response characteristic of HPFRCC. Uniaxial and mesh reinforcements aid in this transition and provide additional resistance to crack opening.

3 UNIAXIAL COMPRESSIVE RESPONSE

3.1 Introduction

Early experimental studies of compressive strength of fiber reinforced cementitious composites using steel, glass and polypropylene fibers (e.g., [27], [28]) suggested that

the influence of fibers on the compressive strength was insignificant at low volume fractions. Both increase and decrease of compressive strength with different fiber types have been experimentally observed (e.g., [29], [30], [31]). Even for the same material, there is mounting evidence that compressive strength may first rise followed by a drop with increasing fiber volume fraction. These observations suggest that the addition of fibers in a cement composite using conventional mixing procedure leads to a competing process of strength improvement as well as degradation. Some recent research, however, suggests that compressive strength can be enhanced substantially even at high fiber volume fraction, when special processing techniques, presumably leading to reduced matrix defects, are employed [32, 33]. Special mix design with high packing density [34] also appears successful in combating defect introduction by fibers. Li and Mishra [35, 36] proposed a simplified micromechanics model to explain the effects of strengthening and weakening of compressive strength of FRC. It is suggested that fibers can lead to higher compressive strengths in HPFRCC in which defects introduction is limited.

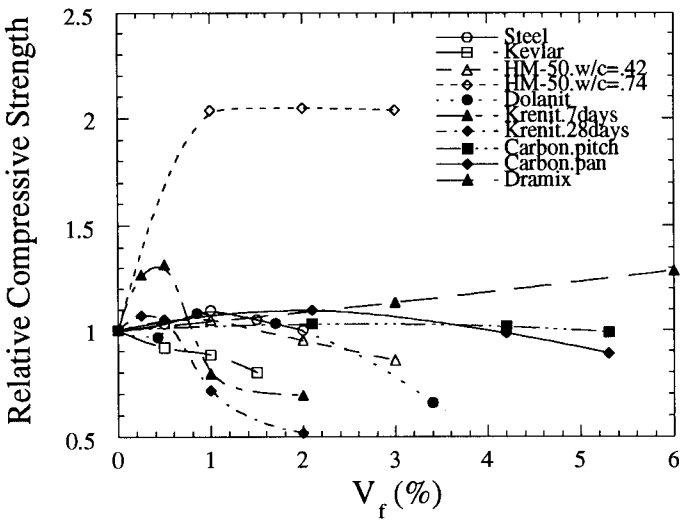

Figure 17. Compressive Strength of Various Fiber Reinforced Cementitious Composites Relative to the Matrix Compressive Strength, as a Function of Fiber Volume Fraction [35].

The proposed model by Li and Mishra is fundamentally based on well known micromechanical models of compressive failure in brittle solids [37, 38, 39]. The influence of fibers on microcrack sliding and extension is based on crack bridging studies carried out in recent years [11, 12]. The model is kept to be as simple as possible in order to obtain close form solutions which elucidate the micromechanical parameters controlling the strengthening and the weakening mechanisms. It is found that depending on the effectiveness and amount of fiber bridging, and the degree to which fibers introduce defects to the composite, both increase and decrease of compressive strength can be derived from increasing fiber content. A summary of

compressive strength change with fiber volume fraction is presented in Fig.17, the details of which can be found in Li [35].

3.2 A Micromechanical Model

Unstable propagation of a critical tensile crack accounts for the failure of brittle solids under tension. However, under compressive loading the microcracks in the solid come under a local tensile field at their tips causing initiation of "wing-cracks" (see Fig.18). The extension of wing-cracks under such a local tension has been demonstrated to be unstable initially and becomes stable as the crack length increases [36, 37]. However presence of other microcracks and the interaction between them induces instability resulting in final failure. When fibers are present in such a body, they affect the crack propagation by increasing the resistance to sliding of the initial microcracks and opening of the wing cracks by crack-bridging. Further, fibers can introduce additional defects, hence high crack density leading to high intensity of crack interaction. These issues will be discussed in the following sections.

3.2.1 Fiber strengthening effect

Resistance to crack-sliding
Based on frictional resistance to the pull out of randomly oriented fibers bridging across a crack (eqn. (7)), Li [35] developed the following equation for reduction in shear stress acting on a sliding crack.

$$\tau_B = \frac{1}{2} s V_f \left(1 - \frac{2a\sigma_c}{L_f G}(1-\mu)(1-\nu) \right) \tag{15}$$

where G and ν are the composite shear moduli and Poisson's ratio respectively, a is the half crack length, and μ is a coefficient of friction against shear sliding of the crack faces. The reinforcement index *s* is defined as

$$s = g\tau \left(\frac{L_f}{d_f} \right) \tag{16}$$

where d_f is the diameter of the fiber and τ is the interfacial shear strength. For typical values of the snubbing coefficient f (associated with inclined fiber pull-out, [13]) ranging from 0 to 1, the snubbing factor g ranges from 1 to 2.3.

The net shear stress acting on the sliding microcrack is therefore given by

$$\tau = \frac{1}{2}\sigma(1-\mu) - \tau_B \tag{17}$$

where the first term on the right hand side represents the shear stress for the most critical sliding crack (oriented at 45^0 to the loading axis, see [36]).

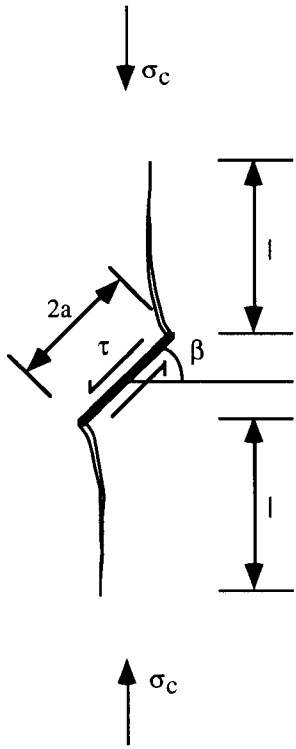

Figure 18. Wing-Crack Growth Induced by Sliding of Microcrack as the Basic Mechanism of Compressive Failure in Brittle Solids [35].

Resistance to wing-crack growth

The wing-crack, like the sliding microcrack, will also be bridged by fibers. As the wing-crack grows, increasing amount of bridging fibers will lead to an increase in crack closing pressure in an enlarging 'process zone'. Based on an R-curve concept associated with fiber bridging, Li [35] developed an expression for the total toughness against which the wing-cracks have to propagate against:

$$K_{IC} = K_m + \sqrt{\frac{l}{l_o^*} E G_o} \tag{18}$$

where K_m is the fracture toughness of the cementitious material without fibers, E and G_o are the composite Young's moduli and the composite fracture energy, respectively and l^* defines the wing-crack length extension at which the linearized R-curve reaches the plateau value for the bridging fracture energy [35]. In the case of FRC, Li [12] found that G_o can be related to the fiber and interfacial properties:

$$G_o = \frac{1}{12} s L_f V_f \tag{19}$$

Assuming that linear elastic fracture mechanics holds on the scale of micro-defects, we can obtain an expression relating the normalized compressive load σ_o required to maintain the normalized wing-crack length l_o:

$$\sigma_o \equiv \frac{\sigma\sqrt{\pi a}}{K_m} = \left\{\frac{B[l_o,\mu,V_f,c]}{A[l_o,\mu,D_o]} + C[K_o,s_o,V_f]\right\}\frac{1}{D[s_o,V_f]} \tag{20}$$

where

$$A[l_o,\mu,D_o] \equiv \frac{1-\mu}{\pi\sqrt{2(l_o+0.27)}} + \frac{\sqrt{2}}{\pi}\sqrt{D_o}\left(l_o+\frac{1}{\sqrt{2}}\right)^{1/2}$$

$$B[l_o,\mu,V_f,c] \equiv (1-\mu)\left\{1+\sqrt{\frac{\bar{a}}{l_o^*}cl_oV_f}\right\}$$

$$C[K_o,s_o,V_f] \equiv \frac{s_oV_f}{K_o}$$

$$D[s_o,V_f] \equiv (1-\mu)\left(1+4(1-\nu^2)s_oV_f\bar{a}\right) \text{ and}$$

D_0 = initial flaw density

and the non-dimensional parameters are defined as:

$$l_o \equiv \frac{l}{a};\ l_o^* \equiv \frac{l^*}{L_f};\ \bar{a} \equiv \frac{a}{L_f};\ s_o \equiv \frac{s}{2E};\ c \equiv \frac{1}{12}\frac{sL_fE}{K_m^2};\ K_o \equiv \frac{K_m}{E\sqrt{\pi a}}.$$

3.2.2 Fiber weakening effect

As mentioned before, the addition of fibers beyond a certain optimal level may adversely affect the compressive strength due to introduction of additional defects and difficulties in processing. To account for this effect Li [35] suggested a simple modification in the initial flaw density or damage index parameter D_0 following experimental observations. By introducing the fiber induced damage index *k*, we redefine D_0 as given by the following equation.

$$D_O = (N_A\pi a^2)\, e^{kV_f} \tag{21}$$

where N_A is defined as the number of cracks per unit area. The parameter *k* is probably dependent upon the fiber type and processing techniques and has to be evaluated by experimental investigation for particular fiber-matrix systems.

Glavind [40] has accounted for fiber induced damage effect in a different manner. Instead of assuming an increase in initial flaw density, the initial flaw size, a, is assumed to change due to the addition of fibers. The proposed damage rule is as follows:

$$a' = a\left[\exp\left(\alpha V_f \frac{L_f}{d_f}\right)\right] \tag{22}$$

where α stands for the damage coefficient to be determined empirically. With properly adjusted α, the composite strength prediction can agree well with experimental data [40]. However, the lack of physical meaning of this parameter has some drawback.

3.3 Combined Strengthening and Weakening Effect of Fiber Addition

Eqns. (20) and (21) may be used to study the effect of fiber on compressive strength in FRCs, when microcrack sliding resistance, wing-crack growth resistance, and damage introduction are operational simultaneously, as is suggested by experimental data such as that shown in Fig.17. Fig.19a shows the normalized compression load required to drive a wing-crack of length l ,for various fiber volume fractions. In Fig.19b, we show that the compressive strength may continue to rise even beyond 4% when the fiber damage index is small (e.g. k = 25), but rapidly drops beyond 0.4% when the fiber damage index is large (e.g. k = 100). In between these extremes, compressive strength is seen to rise initially with fiber volume fraction, and then decreases with additional amount of fibers. These predictions of fiber induced compressive strength changes are in qualitative agreement with the experimental data shown in Fig.17.

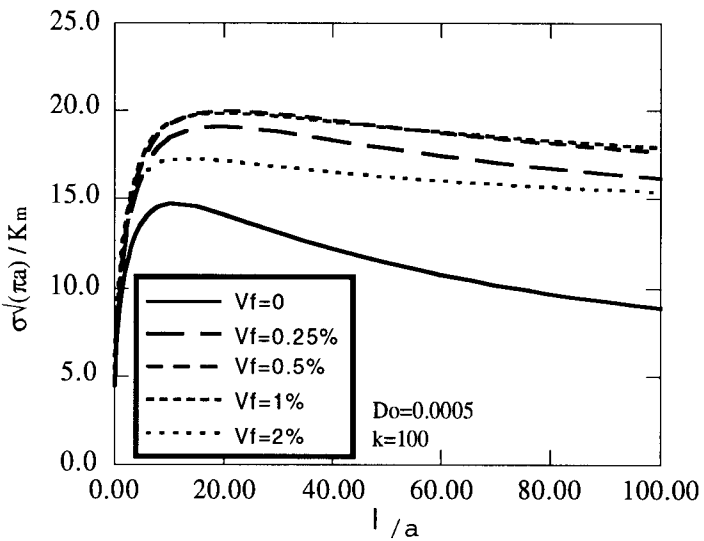

Figure 19a. Combined Strengthening and Damage Effect of Fibers: Normalized Compression Load Required to Drive a Wing-Crack of Length l, for Five Different Fiber Volume Fractions. Parametric Values Used are l_o^* = 20; D_o = 0.0005; = 0.1; c = 800; K_o = 0.0002; s_o = 0.01, and k=100 [36].

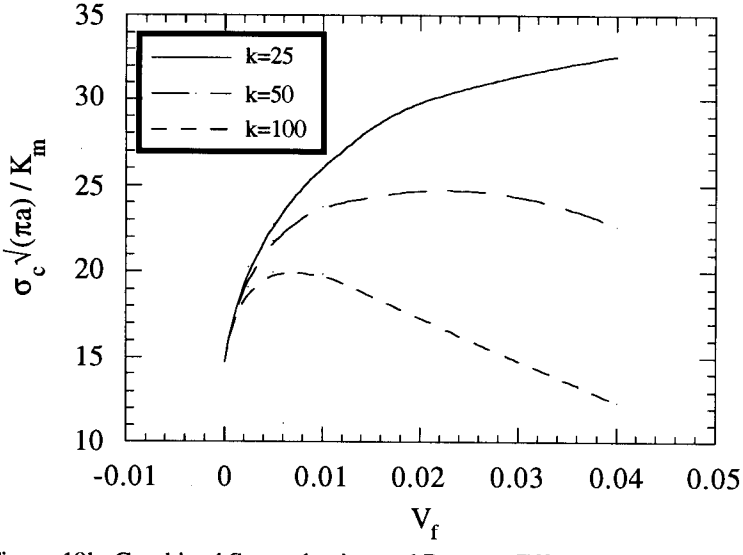

Figure 19b. Combined Strengthening and Damage Effect of Fibers: Predicted Compressive Strength Change with Fiber Volume Fractions, for Different Fiber Induced Damage Index k. Parametric Values Used are $l_o^* = 20$; $D_o = 0.0005$; $\bar{a} = 0.1$; $c = 800$; $K_o = 0.0002$; $s_o = 0.01$ [36].

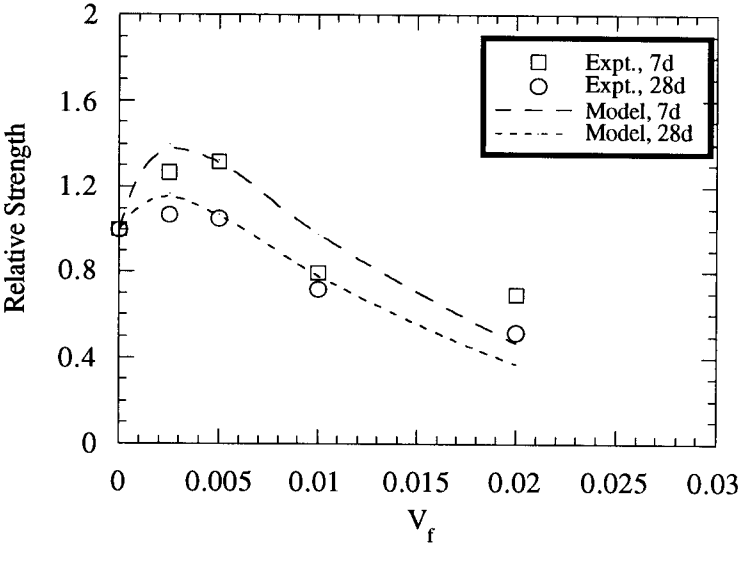

Figure 20. Model Predictions for the Krenit Fiber Reinforced Composite [36].

Fig.20 shows model predictions for the Krenit (a polypropylene) fiber reinforced concrete data (also shown in Fig.17). Common parametric values chosen for both sets of data were discussed by Li and Mishra [36]. Reasonable comparisons can be found between experimental data and theoretical predictions (Fig.20). However, it should be mentioned that there is plenty of uncertainty in the exact parametric values (since they are not measured), although the numbers used should not be too far off.

3.4 Further Discussions and Conclusions

Although the microcrack sliding model of compressive strength in brittle material has been discussed in the context of uniaxial loading in the present treatment, extensive studies [36, 37, 38] have shown that the compressive strength is very sensitive to confining stresses. This can be seen in the sensitivity of the stress intensity factor of the wing-cracks to normal compressive load. This notion is in accord with experience in cementitious materials, for which confinements are general prescriptions to derive higher compressive load bearing capacity. The present model of compressive strength for FRC shows that fibers can be exploited to increase the compressive strength and may therefore act as a passive confining pressure. This passive confinement idea was first proposed by Yin et al [41], who discovered this beneficial effect of fiber in a series of biaxial steel FRC tests.

The present work represents a preliminary look at how fibers in FRC contributes or degrades composite mechanical properties. The results based on the present model appear to capture much of what has been experimentally observed in compressive strength change due to fiber addition. These modelling results (particularly Fig.19) indicate that fibers can significantly improve compressive strength of HPFRCC if the weakening effect of fiber is controlled via novel processing routes. Hence micromechanical models can provide rationale for selection of materials constituents (properties of fiber, matrix, and interface) in design of compressive strength of HPFRCC. Compressive strength itself is not only an important parameter, but also strongly influence the flexural behavior of HPFRCC. More detailed discussed on flexural strength will follow in Section 4. A difficulty in applying the current model, however, lies in the lack of knowledge in some micromechanisms and micromechanical parameters. These include, for example, the detail micromechanisms in the way fiber resist microcrack sliding, and the general unavailability of parametric values of a, D_0, and k. Additional research is required to tackle these issues. The present work provides a framework for which these future research should be organized.

4 FLEXURAL RESPONSE

4.1 Introduction

The flexural strength of unreinforced cement-based materials and their fiber composites is important for many current applications such as road slabs, airfield runways, roofing tiles, sewage pipes, and architectural wall panels. In addition, using a simple flexure test, an important property of cement-based materials, namely their tensile strength, can be deduced from their flexural strength if the latter can be related to the former through an analytical or numerical model.

The flexural strength of cement-based materials is known to depend on their tensile failure mode. Hillerborg et al. [42] and Zhu [43] showed that the flexural strength of concrete depends on a parameter called the brittleness ratio which is a function of material properties and specimen geometry. In particular, they showed that the flexural

strength of concrete depends on the material fracture resistance described by the tension-softening relation (σ–δ) (see e.g. eqn (7)). Babut and Brandt [80] have attempted to account for the effect of adding steel fiber on the flexural behavior of concrete beam. They developed a semi-empirical method based on the classical reinforced beam theory and experimental data. They discovered that the MOR values of steel fiber reinforced concrete (V_f=2%) can be 2-3 times higher than that of plain concrete.

In an un-notched beam specimen made of a quasi-brittle FRCC, first cracking is accompanied by the development of a localized fracture process zone. In this process zone, the bridging fibers can partially transfer the stress across the crack, however, the magnitude of the transferred stress decreases as the crack enlarges. Therefore, no additional cracks will form beyond this first crack. During this process, energy due to fiber frictional pull-out is being consumed. Because of this energy absorption, the flexural strength of regular FRCC is higher than their tensile strength [44]. In contrast, in an un-notched beam specimen made of a strain hardening HPFRCC material, first cracking is accompanied by a strain concentration at the mouth of the crack. Because of the stress transfer capability of the reinforcing fibers in a strain hardening material, stress redistribution will occur so that localized fracture will be delayed. Consequently, an expanded zone of matrix cracking (parallel to the first crack near the tensile face of the beam) must develop prior to localized fracture. Such an extensive volumetric cracking process involves considerable energy absorption which give rise to a high flexural strength (MOR) to tensile (first cracking) strength ratio.

4.2 Flexural Strength of Quasi-brittle FRCC

Maalej and Li [45] studied the flexural strength of quasi-brittle FRCC. In their study, they adopted the fictitious crack model (FCM) concept to relate the flexural strength of these composites to the material's tension softening property and specimen geometry. In prior studies [12, 14], the tension softening relationships for these composites have been related to the material's micromechanical parameters (such as fiber length, fiber diameter, fiber tensile strength, fiber/matrix interfacial bond strength, fiber and matrix elastic moduli) through explicit analytical expressions taking into account the effect of fiber rupture.

Fig.21 shows the distribution of normal stresses in the critical beam section as assumed by Maalej and Li [45]. A fictitious crack of length a and mouth opening w was assumed to form on the beam tensile face. Within the fracture process zone, the stress σ at any point x, was related to the width δ of the fictitious crack at that point by the following tension softening relationship:

$$\sigma(\delta) = T_b\left[1 - 2k\left(\frac{\delta}{w_c}\right) + p\left(\frac{\delta}{w_c}\right)^2\right] \tag{23}$$

Eqn (23) describes the stress-crack width relationship for fiber reinforced composites assuming frictional interfacial bond and modifies eqn (7) by taking into account the effect of fiber rupture [14]. In Eqn (23), w_c represents the crack width at which the bridging stress vanishes, T_b represents the post-cracking strength of the composite, k describes the magnitude of the initial slope of the tension softening curve, and p describes the rate at which the slope of the tension softening curve decreases as a function of crack width. For the simple case of only fiber pull-out in the composite eqn

(23) is reduced to eqn (7) where $\delta_p < \delta < L/2$. The parameters w_c, T_b, k, and p depend on the composite micromechanical parameters as defined in the original papers [12, 14].

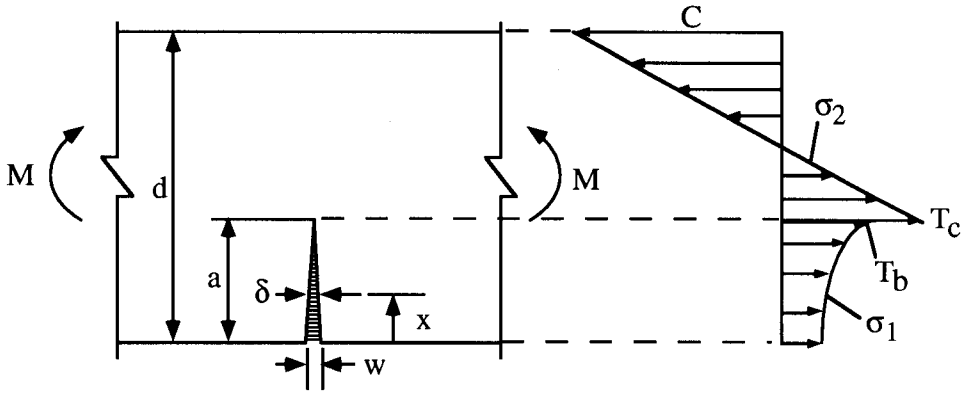

Figure 21. Distribution of Normal Stresses in the Critical Beam Section [45].

The crack was assumed to have a linear profile such that the crack width δ at any location x within the fracture process zone can be related to the crack mouth opening w as follows:

$$\delta = w\left(1 - \frac{x}{a}\right) \tag{24}$$

The hypothesis of the FCM, that the crack propagates as soon as the stress at the crack tip exceeds the tensile strength of the material, was adopted. Furthermore, a linear stress distribution $\sigma_2(x)$ outside the fracture process zone with a maximum tensile stress T_c at the crack tip and a compressive stress C at the beam compressive face was assumed (see Fig.21).

By adopting the above assumptions, Maalej and Li derived an analytical expression for the moment M as a function of the composite micromechanical parameters, specimen geometry, and crack length. It was shown that the moment M reaches a maximum value M_u when the fracture process zone is only partially developed (i.e. $0 < a < d$). The composite flexural strength was computed by the use following equation:

$$MOR = MOR(d, T_c, E_c, V_f, L_f, d_f, \sigma_{fu}, \tau, f) = \frac{6M_u}{bd^2} \tag{25}$$

Maalej and Li [45] showed that the ratio of flexural strength to tensile strength varies as a function of the brittleness ratio B defined in their study as $(T_b d)/(E_c w_c)$, where E_c is the elastic modulus of the composite. It was shown that the ratio of flexural strength to tensile strength decreases with increasing brittleness ratio. In the limiting case when B is infinite, corresponding to linear elastic brittle behavior of the material, the flexural strength is equal to the tensile strength as predicted by the linear elastic brittle theory.

In the other limiting case, $B \rightarrow 0$, the ratio of flexural strength to tensile strength is equal to 3, as predicted by elastic perfectly plastic theory.

Fig.22 shows the variation of the flexural strength to tensile strength ratio q_u as a function of fiber length for a typical fiber reinforced composite. This figure indicates that q_u increases initially as a function of fiber length, reaches an optimum value, and then starts to decrease as the fiber length continues to increase. The drop in q_u is due to fiber rupture which reduces the stress acting across the fracture process zone. Alternatively, the energy consumed due to fiber frictional pull-out is known to diminish with fiber length when fiber rupture occurs. Therefore, it is deduced that an optimum fiber length exists at which the ratio of flexural strength to tensile strength is optimum.

Fig. 22 may also be useful to interpret time-dependence of MOR observed in some FRC. For example, Bentur and Katz [46] found that CFRC reach a peak in q_u, afterwhich the MOR drops. In this case, L_f is fixed, but τ and therefore $L_f/2L_c$ is expected to be a increasing function of time.

The model proposed by Maalej and Li [45] can be used to predict the flexural strength of any quasi-brittle fiber reinforced cementitious composite based on the knowledge of either its micromechanical parameters or its tension softening relationship. In addition, the model can be used to perform a parametric study on the flexural strength of any fiber reinforced composite. This allows an understanding of how the flexural strength of fiber reinforced composites depends on the different micromechanical parameters, so that the flexural strength can be controlled by the micromechanical parameters.

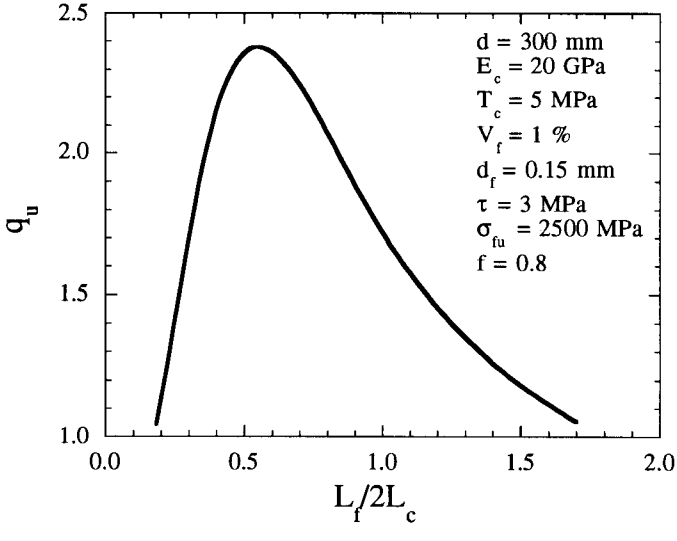

Figure 22. Variation of Flexural Strength to Tensile Strength Ratio as a Function of Fiber Length [45].

Fig.23 shows the variation of flexural strength as a function of beam depth, as predicted by the above model and experimentally measured by Ward and Li [44] for a

6.4 mm aramid fiber reinforced mortar. The fiber volume fraction was 1.5 percent, and the beam depths were 63.5, 114, 171, and 228 mm. The critical fiber length for this composite is 3.6 mm. This indicates that the composite must have failed with a large fraction of ruptured fibers within the beam fracture process zone. Fig.23 shows that there is a reasonable agreement between the experimental data and the theoretical prediction for the composite flexural strength. The model and experimental data suggest that the flexural strength decreases as the depth of the beam increases. This size effect of decreasing flexural strength with increasing beam depth has also been experimentally recorded for plain concrete (e.g. [42], [47]) and fiber reinforced concrete (e.g. [48]). Thus even though MOR is often regarded as a material property, element size-effect must be accounted for in safe design of structures. Due to fiber reinforcement, however, size effect is less severe in FRCC than in plain concrete structural elements.

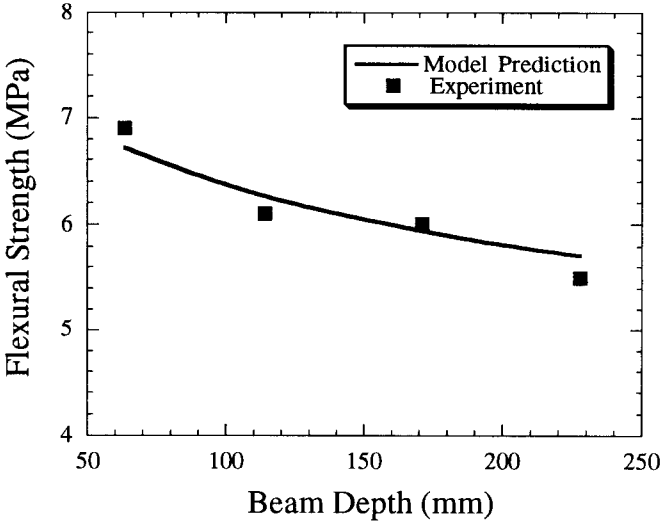

Figure 23. Effect of Beam Depth on Flexural Strength of Aramid Fiber Reinforced Mortar (L_f = 6.4 mm, d_f = 0.012 mm, σ_{fu} = 2800 MPa, τ = 4.5 MPa, f = 0.95, T_c = 4.6 MPa, E_c = 20 GPa) [45].

4.3 Flexural Strength of Strain-Hardening FRCC

Maalej and Li [49] studied the flexural behavior of strain hardening FRCC (hereafter referred to as HPFRCC) where the reinforcing fibers are discontinuous and randomly distributed in the matrix. These composites have been designed according to micromechanical models (Eqn (9)) which are constructed on the basis of micro-mechanics of defect growth in a brittle matrix composite whereby crack bridging is provided by fibers to achieve steady state cracking [1, 10]. This design principle is detailed in sections 2.3 and 2.4. The flexural behavior of HPFRCC was related to their uniaxial compressive and tensile stress-strain behavior. The HPFRCC material was assumed to exhibit a strain hardening behavior characterized by the stress-strain curves shown in Fig.24a and 24b for uniaxial tension and compression, respectively. To simplify the analysis, it was assumed that the stress-strain behavior of the HPFRCC

material in uniaxial tension and compression can be described by bilinear stress-strain curves as shown in solid line in Fig.24a and 24b, respectively. In a rectangular beam, having a width b and depth d, the strain was assumed to vary linearly along the beam's depth. This results in the stress distribution shown in Fig.25 for the portion of the beam subjected to the highest bending moment M. It was assumed that prior to reaching the ultimate bending moment M_u, an inelastic microcracking zone of size a expands from the extreme tensile fiber towards the extreme compressive fiber.

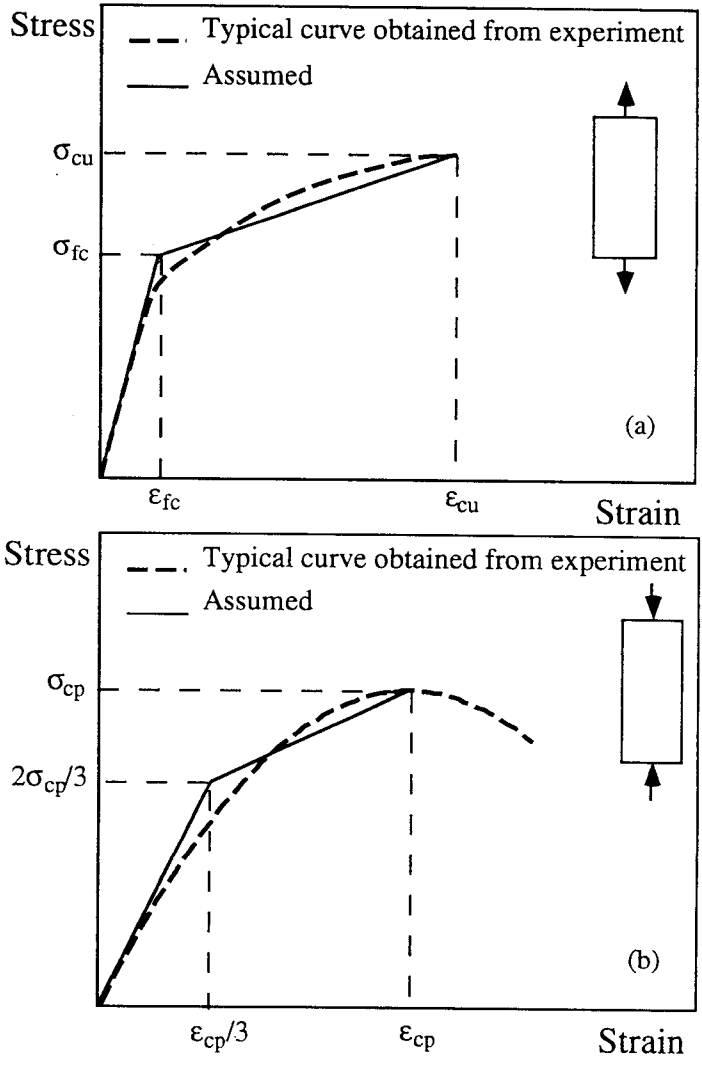

Figure 24. Stress-Strain Behavior of HPFRCC (a) Uniaxial Tension (b) Uniaxial Compression [49].

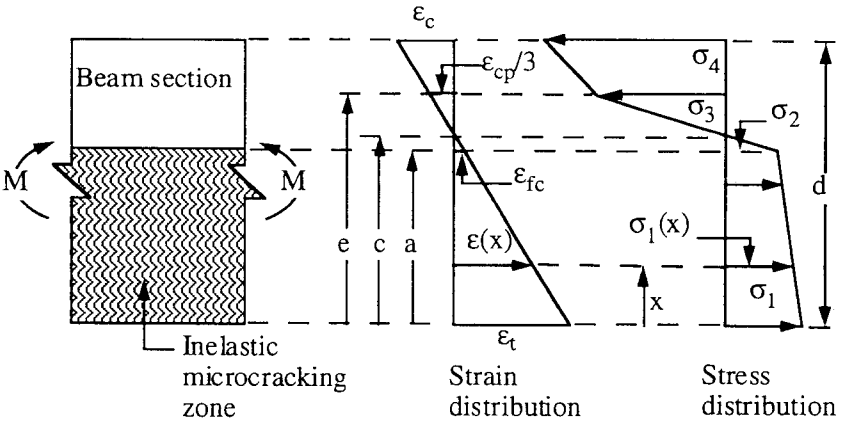

Figure 25. Strain and Stress Distribution along the Beam Depth [49].

Maalej and Li [49] derived an analytic expression for the external bending moment M as functions of the known material parameters, specimen dimensions, and the size of the microcracking zone:

$$M = M[\sigma_{fc},\varepsilon_{fc},\sigma_{cu},\varepsilon_{cu},\sigma_{cp},\varepsilon_{cp},a,b,d] \tag{26}$$

where σ_{fc} is the tensile first cracking strength, ε_{fc} is the tensile first cracking strain, σ_{cu} is the ultimate tensile strength, ε_{cu} is the ultimate tensile strain, σ_{cp} is the compressive strength, ε_{cp} is the compressive strain at peak stress, and a is the depth of inelastic microcracking zone. Material properties such as σ_{fc} , ε_{fc}, σ_{cu}, ε_{cu}, and σ_{cp} have already been related to the composite micromechanical parameters through explicit analytical expressions [1, 12, 14, 34].

It was assumed that the beam fails when the applied moment M is equal to the ultimate moment capacity of the beam M_u. Furthermore, it was assumed that the beam fails by exhausting the strain-capacity of the material either at the tensile face ($\varepsilon_t > \varepsilon_{cu}$) or at the compressive face ($\varepsilon_c > \varepsilon_{cp}$).

The flexural stress corresponding to M and the modulus of rupture (MOR) corresponding to M_u are given by:

$$\sigma_f = \frac{6M}{bd^2} = \sigma_f[\sigma_{fc},\varepsilon_{fc},\sigma_{cu},\varepsilon_{cu},\sigma_{cp},\varepsilon_{cp},r] \tag{27}$$

$$MOR = \frac{6M_u}{bd^2} = \sigma_f[\sigma_{fc},\varepsilon_{fc},\sigma_{cu},\varepsilon_{cu},\sigma_{cp},\varepsilon_{cp},r_u] \tag{28}$$

where r = a/d, and r_u correspond to the size of the microcracking zone when the ultimate moment capacity of the beam is reached.

Based on geometrical considerations, the beam curvature was computed as the ratio of strain in the extreme tensile fiber (ε_t) to the distance from the extreme tensile fiber to the neutral axis (c):

$$\frac{1}{\rho} = \frac{\varepsilon_t}{c} \tag{29}$$

For a constant curvature, the maximum deflection for a beam having a span L is given by:

$$u = \frac{L^2}{8\rho} \tag{30}$$

Maalej and Li [49] showed that the moment-curvature (or flexural stress-curvature) diagram of a beam can be computed by using Equations (26) and (29) [or (27) and (29)] and allowing r to vary between 0 and r_u.

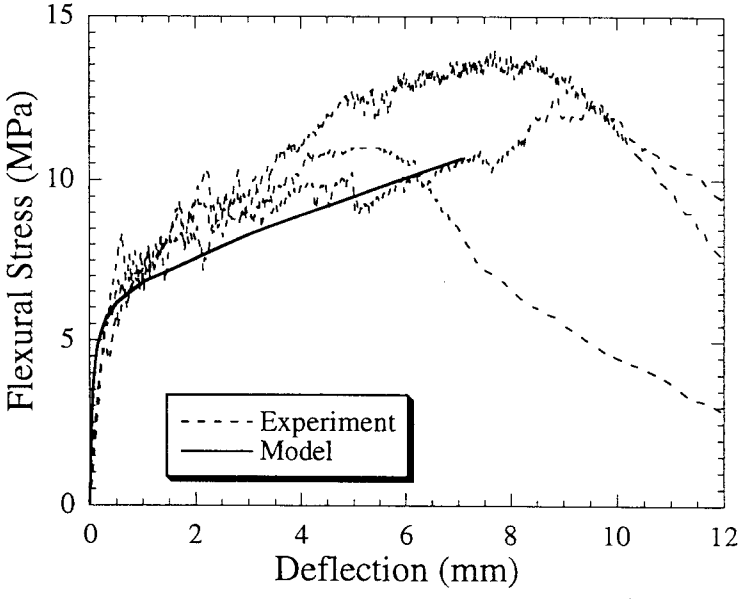

Figure 26. Comparison Between Predicted and Experimentally Measured Flexural Stress-Deflection Curves for the 2% Polyethylene HPFRCC (σ_{fc} = 2.5 MPa, ε_{fc} = 0.00021, σ_{cu} = 4.6 MPa, ε_{cu} = 0.056, σ_{cp} = 60 MPa, ε_{cp} = 0.01, d = 101.6 mm) [49].

Fig.26 shows a comparison between a predicted flexural stress-deflection curve and that experimentally measured for a third-point bending specimen made of an HPFRCC material. The depth of the specimen and the tensile and compressive properties of the HPFRCC material used in the computation are also shown in Fig.26. In computing the

model predicted beam deflection, it was assumed that the curvature is approximately constant along the length of the beam and equal to the curvature at the middle span. Interpretation of the computations which led to Fig.26 indicates that first cracking occurs when the flexural stress in the beam is equal to 2.5 MPa. Then the microcracking zone (of size a) starts to move up from the extreme tensile fiber toward the extreme compressive fiber. At the same time the position of the neutral axis is moving away from the centroid of the beam cross-section toward the extreme compressive fiber. This is accompanied by a continuous decrease in the stiffness of the beam. Initially, the compressive stress distribution within the beam is linear. After a certain propagation of the microcracking zone, the compressive stress distribution becomes bilinear. The maximum moment is reached when the tensile strain in the extreme tensile fiber reaches the ultimate tensile strain of the HPFRCC material. At that moment, the size of the microcracking zone (a) is about 90 % of the beam depth. As shown in Fig.27 this result is consistent with the experimentally observed microcracking zone size around the peak load.

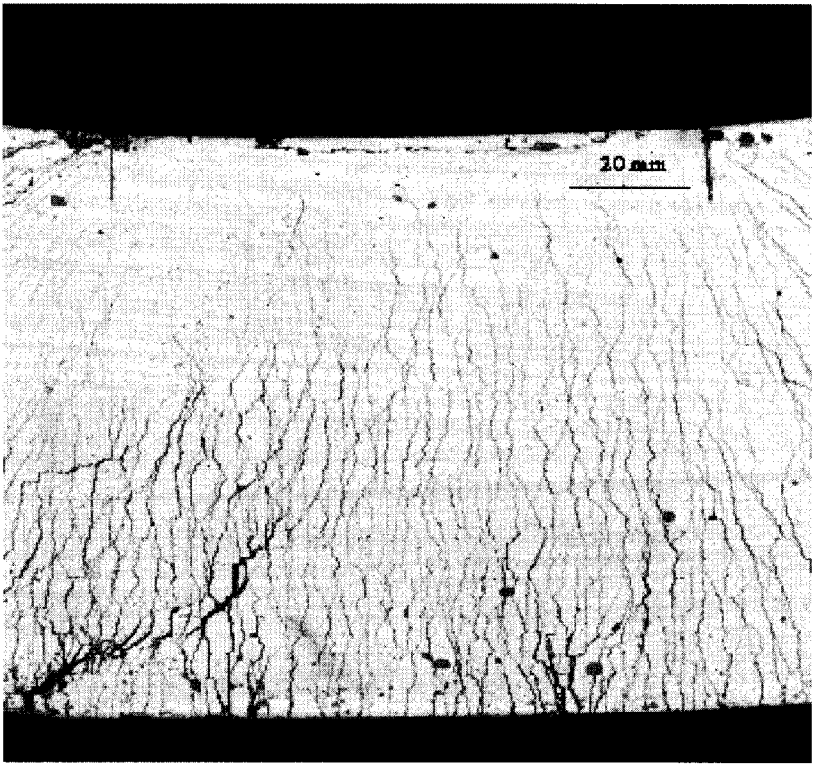

Figure 27. Cracking Pattern in the Beam Middle Span Around the Peak Load [49].

The above model suggests that the flexural strength of HPFRCC materials can be increased by increasing the strain capacity, the tensile first cracking strength, and/or the ultimate tensile strength of the material. The results of this model can be used in conjunction with micromechanical models of tensile properties of HPFRCC materials to optimize their flexural strength. Li et al. [50] showed that the tensile first cracking strength, the ultimate tensile strength, and the ultimate tensile strain can be increased

while maintaining a low fiber volume fraction by proper tailoring of the micromechanical parameters (fiber, matrix, and fiber/matrix interface properties) according to micromechanical models constructed on the basis of fracture mechanics and deformation mechanisms.

Maalej and Li [49] showed that the MOR/σ_{fc} ratio in HPFRCC is greater than three and can be as large as five as demonstrated in the 2% polyethylene HPFRCC. In contrast, for quasi-brittle materials, the ratio of flexural strength to tensile strength has an upper bound of three. This results shows the importance of achieving strain hardening behavior in FRCC. To further clarify this point, let's assume that a 2% FRCC shows a quasi-brittle behavior such that the first crack strength is equal to the ultimate strength and equal to 3 MPa. A typical MOR value for this fiber composite can range between 5 and 8 MPa depending the tension softening curve of the material but no more than 9 MPa. Further, let's assume that the micromechanical parameters (L_f, d_f, E_f, σ_{fu}, τ, f; V_f remains 2%) were tailored such that this fiber composite achieved strain hardening behavior with a first crack strength of still 3 MPa, and an ultimate strength of 5 MPa. In this case it is expected that the MOR of this material would be at least 9 MPa, but it could be as high as 15 MPa depending on its ultimate strain capacity. Therefore, by modifying the failure mode of the fiber composite (from quasi-brittle to strain-hardening) an improvement in the tensile strength capacity as well as the MOR would be achieved.

4.4 Conclusions

Fiber reinforcements can be effective in improving flexural strength and flexural ductility in cementitious materials. In FRCC, MOR enhancement is achieved by stabilization of matrix macroscopic crack, basically by the tension-softening branch of the $\sigma-\delta$ curve. This results in MOR to tensile strength ratio of typically 2-3. In HPFRCC, MOR enhancement is achieved by delocalization of damage initiated on the tensile side of the beam, with fibers contributing to this effect via the rising branch of the $\sigma-\delta$ curve. This results in MOR to tensile strength ratio of typically more than 3. In both cases, the size effect of MOR can be drastically reduced. This section highlights the dependencies of bending response on fiber, matrix and interface parameters via micromechanical models. It illustrates that MOR beam size effect, and possibly time-dependency of MOR can be predicted.

5 FRACTURE RESPONSE

5.1 Introduction

One way of overcoming the brittleness of unreinforced cementitious materials is by introducing fibers in the matrix. It has been convincingly demonstrated that significant toughness enhancement can be obtained by proper fiber reinforcement of the cementitious matrix. However, the increased toughness is generally associated with an increase in the overall cost of the material due mainly to the added cost of the fibers and further material processing. To use the minimum amount of fibers and achieve maximum toughness improvement, researches have been developing analytical tools to optimize the design of these fiber composites. The fracture energy due to bridging of discontinuous aligned fibers in brittle matrix composites was studied by Cottrell [51], Cooper and Kelly [52], and Kelly and Macmillan [53], and that of discontinuous randomly distributed fibers was studied by Visalvanish and Naaman [54], Li [12], and Maalej et al [14]. An overview of the above research work is presented in this section.

5.2 Discontinuous-Aligned-Fiber Composites

Assuming a purely frictional fiber/matrix interface, where the shear stress is maintained through-out the fiber pull-out process, Cooper [52] and Kelly and Macmillan [53] derived analytical expressions for the fracture energy G_c due to the bridging of aligned, rigid, and discontinuous fibers in brittle matrix composites. Cooper [52] identified the existence of a critical fiber length l_c beyond which fiber rupture can take place in the composite. He showed that when the fiber length is less than l_c, all fibers will be pulled-out and the fracture energy increases as the square of the fiber length. However, when the fiber length is greater than l_c, some fibers will be ruptured and do not contribute to the fracture energy. In the latter case, Kelly and Macmillan [53] showed that the fracture energy is inversely proportional to the fiber length.

$$\hat{G}_c = \frac{2}{3}\begin{cases} \tilde{L}_f^{\,2} & \text{for } L_f < 2L_c \\ \tilde{L}_f^{\,-1} & \text{for } L_f \geq 2L_c \end{cases} \tag{31}$$

where $\hat{G}_c = G_c/G_o$, $G_o = V_f \tau L_c^{\,2}/d_f$, $L_c = \sigma_{fu} d_f/4\tau = l_c/2$, and $\tilde{L}_f = L_f/2L_c$.

In the above equation, and σ_{fu} is the tensile rupture strength of the fiber.

According to Cotterell [51], the fracture energy can be maximized by increasing the critical fiber length l_c and keeping the fiber length closely equal to l_c. When L_f is equal to l_c, the fracture energy G_c is at an optimum value given by the following equation:

$$G_c^{opt} = \frac{2}{3}\frac{V_f \tau L_c^{\,2}}{d_f} = \frac{1}{24}\frac{V_f \sigma_{fu}^{\,2} d_f}{\tau} \tag{32}$$

Therefore G_c^{opt} can be maximized by increasing the strength of the fiber, increasing the diameter of the fiber, and/or decreasing the fiber/matrix interfacial bond strength. All of these effects amount to increasing the critical fiber length l_c.

5.3 Discontinuous-Randomly-Distributed-Fiber Composites

The fracture energy due to bridging of discontinuous randomly distributed fibers in brittle matrix composites can be computed by integrating the area under the composite bridging stress-displacement (σ-δ) curve [12, 54] (see eqns. (7) and (23)). The area under the pre-peak σ-δ curve represents the fracture energy absorbed during the fiber debonding process, and the area under the post-peak σ-δ curve represents the fracture energy absorbed during the fiber pull-out process.

5.3.1 Pull-out Fracture Energy

Assuming a purely frictional fiber/matrix interface and complete fiber pull-out, Visalvanich and Naaman [54] derived a semi-empirical model for the tension softening curve (σ-δ) in discontinuous randomly distributed steel fiber reinforced mortar. From the derived σ-δ relationship, and assuming a parabolic crack profile, Visalvanish and Naaman [54] derived an expression for the apparent critical fracture energy G_a of the material:

$$G_a = \alpha\tau V_f \frac{L_f}{d_f}\beta c^n\left[1-1.9\left(\frac{\beta c^n}{L_f}\right)+1.067\left(\frac{\beta c^n}{L_f}\right)^2+0.2\left(\frac{\beta c^n}{L_f}\right)^3\right] \le G_c \qquad (33)$$

where α is the efficiency factor of discontinuous fibers which depends on fiber orientation and average pull-out length of the fiber after matrix cracking, β and n are parameters that define the crack profile, c is a crack extension beyond an initial crack length a_o, and G_c is the steady state fracture energy which can be obtained by integrating the area under the σ-δ curve or by substituting $L_f/2$ for βc^n in eqn (33). In this case the fracture energy would be equal to

$$G_c = 0.171\alpha\tau V_f \frac{L_f^2}{d_f} = G_o\left[0.684\alpha\tilde{L}_f^2\right] \qquad (34)$$

For a linear crack profile n would be equal to 1 and β would be equal to the tangent of the critical crack opening angle CCOA (opening angle of a crack at the onset of its propagation).

Li [12] derived an expression for the composite fracture energy G_c by integrating the area under the post-peak σ-δ curve given by eqn (7). This led to the following expression:

$$G_c = \frac{1}{12} g\tau V_f \frac{L_f^2}{d_f} = G_o\left[\frac{1}{3} g\tilde{L}_f^2\right] \qquad (35)$$

Note that when there is no snubbing effect (i.e. g = 1 corresponding to f = 0), the fracture energy as given by eqn (35) is equal to half the fracture energy as given by eqn (31). This means that the random distribution of fibers reduces the fracture energy by a factor of 2. For some fiber composites, however, this reduction in fracture energy due to the fiber random distribution is offset by the snubbing effect. For instance, polypropylene and nylon fibers in mortar show snubbing factors (g) of 1.8 and 2.3, respectively [13].

The model derived by Li [12] would be identical to the one derived by Visalvanich and Naaman [54] if we set the snubbing factor g equal to approximately 2α.

In eqns (33)-(35), it was assumed that stresses in loaded fibers never reach their tensile rupture strength σ_{fu}. However, it is reasonable to assume that for certain fiber/matrix systems, the combination of fiber embedment length, diameter, inclined angle, interfacial bond, and snubbing friction may lead to stresses in a number of loaded fibers exceeding their tensile strength. In this case, those fibers are expected to break. Li et al. [55] studied the fracture energy associated with fiber bridging in short random fiber reinforced brittle matrix composites taking into account the effect of fiber tensile rupture. They showed that the composite bridging fracture energy can be computed by summing the energy contributions of the individual fibers which bridge the matrix crack plane. This method was later adopted by Maalej et al [14] to drive an analytical expression for G_c that accounts for fiber tensile rupture. Maalej et al [14] assumed that in a composite where potential fiber rupture can occur, all fibers are identical and have

uniform tensile strength along their length. In this case, when fiber rupture occurs, it would be at the matrix crack plane. Therefore, when a fiber breaks, it no longer contributes to the composite fracture energy. Maalej et al [14] identified the existence of a critical fiber length $L_r = 2L_c e^{-f\pi/2}$ beyond which fiber rupture starts to occur in the composite. The composite bridging fracture energy derived by Maalej et al [14] is given by

$$\hat{G}_c = \frac{1}{3}\begin{cases} g(\Phi_b)\tilde{L}_f^{\,2} + h(\Phi_b)\tilde{L}_f^{\,-1} & \text{for } L_r \le L_f < 2L_c \\ g_2\tilde{L}_f^{\,-1} & \text{for } L_f \ge 2L_c \end{cases} \tag{36}$$

where

$$h(\Phi_b) = \frac{1}{2\left(1+f^2\right)}\left[\left(f\sin 2\Phi_b + \cos 2\Phi_b\right)e^{-2f\Phi_b} + e^{-f\pi}\right]$$

$$g(\Phi_b) = \frac{1}{4+f^2}\left[\left(f\sin 2\Phi_b - 2\cos 2\Phi_b\right)e^{f\Phi_b} + 2\right]$$

$$\Phi_b = -\frac{1}{f}\ln\left(\frac{L_f}{2L_c}\right)$$

$$g_2 = \frac{1}{2\left(1+f^2\right)}\left[1+e^{-f\pi}\right]$$

The parameter Φ_b is a critical fiber inclination angle ($0 \le \Phi_b \le \pi/2$) that separates two groups of fibers. Those oriented at an angle less than Φ_b (i.e. $0 \le \Phi \le \Phi_b$) pull-out subsequent to complete debonding, and those oriented at an angle greater than Φ_b (i.e. $\Phi_b \le \Phi \le \pi/2$) could rupture after incomplete debonding if their embedment length is greater than a critical value ($l_u = L_c\, e^{-f\Phi}$). Note that the expression for G_c derived by Li [12] for the case of complete fiber pull-out in the composite is retrieved from eqn (36) by setting $\Phi_b = \pi/2$. In addition, for $L_f \ge 2L_c$ and when there is no snubbing effect (i.e. $g_2 = 1$ corresponding to $f = 0$), the fracture energy as given by eqn (36) is equal to half the fracture energy as given by eqn (31). Once again we verify that the random distribution of fibers reduces the fracture energy by a factor of 2.

As it has been reported for the case of discontinuous aligned fiber composites, eqns (35)-(36) indicate that when the reinforcing fibers are short ($L_f < L_r$) the composite fracture energy is proportional to the square of fiber length, however, when the reinforcing fibers are long ($L_f > 2L_c$) the composite fracture energy is inversely proportional to the length of the fiber. This dependence is depicted in Fig.28 which shows that the fracture energy increases initially as a function of fiber length, reaches a maximum value, and then starts to decrease. Therefore, there exists an optimum length of the fiber at which the fracture energy is maximum. The optimum fiber length and fracture energy are given by the following equations:

$$L_f^{opt} = 2L_c e^{-0.56\sin(f\pi/3)} \tag{37}$$

$$G_c^{opt} = 0.3281\, e^{-1.0532f}\, G_o \tag{38}$$

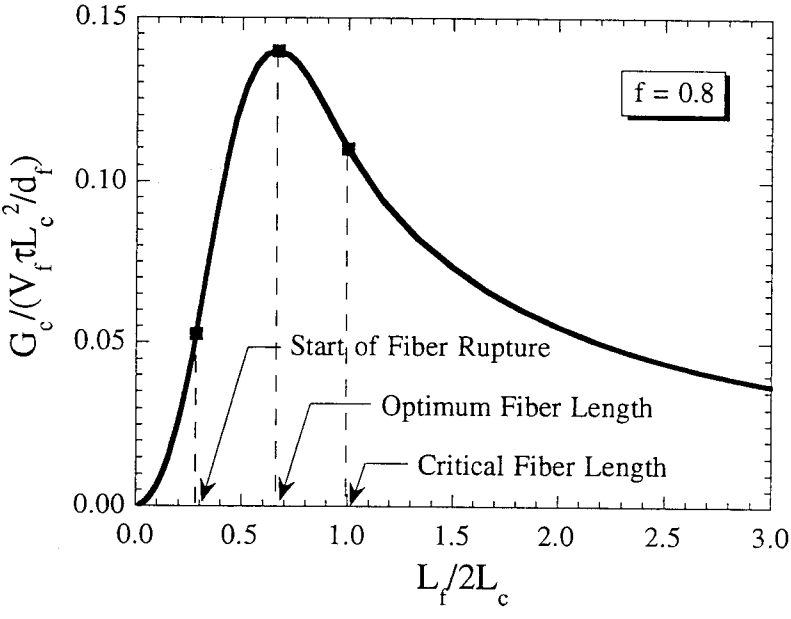

Figure 28. Effect of Fiber Length on Composite Fracture Energy [14].

Eqn (38) indicates that the composite fracture energy can be enhanced by increasing the fiber diameter, decreasing the bond strength, increasing the fiber strength, and/or reducing the snubbing effect. In either case, the optimum fiber length will be increased. However, if the optimum fiber length is to be used in a composite, material processing can become laborious as longer fibers are generally more difficult to process. When there is no snubbing effect (i.e. f = 0), the optimum fiber length would be equal to $2L_c$ as for the case of discontinuous aligned fiber composites. However, G_c^{opt} would be equal to half the optimum fracture energy for discontinuous aligned fiber composites.

Fig.29 shows a comparison between model predicted and experimentally measured composite fracture energy for eight different fiber cement composites. The normalizing micromechanical parameters are listed in Table 1. The data for the steel, polyethylene, and Kevlar fiber composites have been reported by Visalvanich and Naaman [56], Wang et al [57], and Maalej et al [14], respectively. As indicated there is a good agreement between the model predictions and the experimental measurements. Note that for the steel and polyethylene fiber composites no fiber rupture has been reported. However, for the Kevlar fiber composite, fiber rupture has been experimentally observed. This is consistent with the model prediction as shown in Fig.29.

For any conventional fiber reinforced composite, it is possible to alter the micromechanical parameters such that the composite can show a better performance in terms of fracture energy. Whether the composite can be made to achieve its optimum

properties depends on the feasible range of the micromechanical parameters, given the state of technology. For instance, fiber length can be easily customized and controlled. However, material processing can become a problem when long fibers are required for optimum performance. Furthermore, the fiber/matrix interfacial bond strength can be adjusted through, for instance, surface finish modification and/or mechanical crimping [58, 59].

Table 1. Micromechanical Parameters of the Different Fiber Composites.

Fiber	V_f	L_f (mm)	d_f (mm)	L_f/d_f	σ_{fu} (MPa)	τ (MPa)	f
Steel	0.01	6.35	0.150	42	2500	4	1
Steel	0.005	6.35	0.150	42	2500	4	1
Steel	0.02	6.35	0.150	42	2500	4	1
Steel	0.01	12.7	0.150	85	2500	4	1
Steel	0.01	19.05	0.400	48	2500	4	1
Polyethylene	0.01	12.7	0.038	334	2700	1	0.55
Polyethylene	0.006	6.35	0.038	167	2700	1	0.55
Kevlar	0.02	12.7	0.012	1058	3310	4.5	0.6

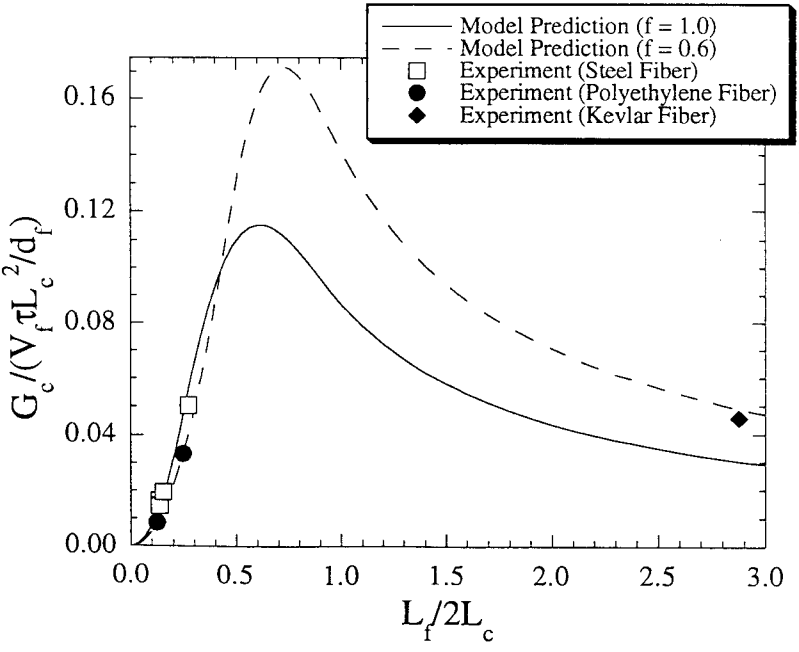

Figure 29. Variation of Composite Fracture Energy as a Function of Fiber Length: Model Prediction vs. Experimental Measurement [14].

5.3.2 Debonding Fracture Energy

Li [12] showed that the fracture energy absorbed during the debonding of discontinuous randomly distributed fibers from the matrix can be estimated by integrating the area under the pre-peak σ_c-δ curve. The result is given by the following equation:

$$G_r = \frac{5}{12}\frac{gV_f\tau^2L_f^3}{d_f^2E_f(1+\eta)} \tag{39}$$

Note that the above equation assumes no fiber rupture in the composite. Comparison between eqns (39) and (35) indicates that the debonding fracture energy is negligibly small with respect to the pull-out fracture energy. Nevertheless, the debonding fracture energy is an important material property that governs the presence or absence of steady state cracking in the composite. Li and Leung [1] showed that to achieve steady state cracking in a composite, it is necessary that the debonding fracture energy is greater than ten time the crack tip fracture energy. For that it is interesting to note that G_r is proportional to the cubic power of fiber length and square power of bond strength, and inversely proportional to the square power of fiber diameter. Therefore, steady state cracking can be effectively promoted by increasing the fiber length, increasing the bond strength, and/or reducing the fiber diameter.

The dependence of G_r on the micromechanical parameters (particularly L_f, τ, and d_f) is altered as fiber rupture starts to occur in the composite ($L_f > L_r$). When fiber rupture occurs in the composite G_r would be equal to:

$$G_r = \frac{1}{12}\frac{gV_f\tau^2L_f^3}{d_f^2E_f(1+\eta)}\left[8\left(\frac{L_r}{L_f}\right)^3 - 3\left(\frac{L_r}{L_f}\right)^4\right] \tag{40}$$

It can be shown that the debonding fracture energy in the case of fiber rupture can be increased by increasing the length of the fiber, increasing the strength of the fiber, increasing the diameter of the fiber, reducing the interfacial bond strength, reducing the elastic modulus of the fiber, and/or reducing the snubbing factor.

5.4 Strain Hardening Cementitious Composites

A ductile fracture mode has been recently reported by Li and Hashida [60] in a double cantilever beam fracture specimens fabricated from a cement paste matrix reinforced with 2% by volume of polyethylene fibers. The recorded fracture behavior was characterized by the development of an off-crack-plane microcracked zone in addition to the bridging process zone observed in quasi-brittle fracture mode. The areal dimension of this inelastic damage zone was observed to be more than 500 cm^2 leading to an extensive off-crack-plane inelastic energy absorption. The total fracture energy consumed in the fiber bridging fracture process zone, and in the inelastically deformed material off the crack plane, was measured to be 24 kJ/m^2. This ductile fracture phenomenon was made possible by the strain hardening behavior of the composite material. Kabele and Horii [61] proposed a simple analytical model for fracture analysis of strain hardening FRCC (hereafter referred to as HPFRCC). The model was used to predict the fracture energy of the composite based on the knowledge of the uniaxial tensile behavior of the material. In this model, the composite undergoing multiple

cracking was treated as a homogeneous continuous material with additional strain, called inelastic cracking strain, which represents the crack density and opening. The strain-hardening theory of plasticity was used to model the multiple cracking in HPFRCC. The authors used the associated flow rule and a yield function where the yield surface in 2-D stress state is defined by the following function:

$$F \equiv \frac{\sigma^*_{xx} + \sigma^*_{yy}}{2} + \sqrt{\left(\frac{\sigma^*_{xx} - \sigma^*_{yy}}{2}\right)^2 + \left(\frac{\sigma^*_{xy} - \sigma^*_{yx}}{2}\right)^2} - \sigma_{fc} = 0 \qquad (41)$$

where σ^*_{xx}, σ^*_{yy}, σ^*_{xy}, and σ^*_{yx} are initially equal to the in-plane components of the stress tensor and σ_{fc} is the first cracking strength (see section 2.3 and 2.4). Note that this model accounts for the fact that multiple cracking is initiated on planes normal to the direction of the maximum principle stress. This implies that at any point of the material, multiple cracking can evolve in any direction according to the local stress field.

Pseudo-strain hardening during multiple cracking was represented by the following kinematic hardening rule:

$$\sigma^*_{ij} = \sigma_{ij} - \alpha_{ij} \qquad (42)$$

where ij equals to xx, yy, xy, and yx; σ_{ij} are components of the stress tensor; and α_{ij} are defined by:

$$d\alpha_{ij} = h\, d\varepsilon^c_{ij} \qquad (43)$$

where $d\varepsilon^c_{ij}$ are components of the incremental cracking strain tensor and h is a material parameter associated with the tangent of the σ–ε relation in the strain-hardening regime.

In the model above for multiple cracking, the cracking strain characterize the crack openings smeared over the material volume. Thus, the direction of the maximum principle cracking strain is normal to the direction of the most developed cracks. Consequently, the condition for crack localization is defined as follows: a localized crack is formed on the plane normal to the maximum principle cracking strain when its magnitude reaches certain critical value $\varepsilon_{cu}{}^*$.

Localized cracks are modeled as discrete discontinuities in the displacement field and the effect of fiber bridging is represented by a traction applied to the crack surfaces. The magnitude of this traction decreases with increasing normal COD according to the tension softening relationship:

$$dt_n = s\, d\delta_n \qquad (44)$$

where dt_n is the incremental normal traction, s is the slope of the tension softening curve, and $d\delta_n$ is the incremental normal COD. The material parameters σ_{fc}, h, ε_{cu}^*, and s are determined from the uniaxial tensile test.

Kabele and Horii [61] implemented the above model into a FEM code, and attempted to reproduce the results of experiments conducted on HPFRCC by Li and Hashida [60] and Maalej et al [14]. In the former study, Li and Hashida [60] used the J-based technique to measure the fracture energy of a strain hardening polyethylene fiber reinforced cement paste where the fiber volume fraction was 2%. The bridging fracture energy was measured by integrating the area under the post-peak stress-displacement curve obtained from a uniaxial tensile test. The total fracture energy was measured using load displacement curves of two DCB specimens which differ only in the original notch length.

Kabele and Horii [61] determined the material parameters for the model from the uniaxial tensile stress-strain curve as shown in Fig.30. Using these parameters, they analyzed the DCB specimens. The FEM mesh used consisted of 2530 isoparametric quadrilateral 4-node elements. During the computation some of these elements were changed into cracked elements due to the localized crack propagation.

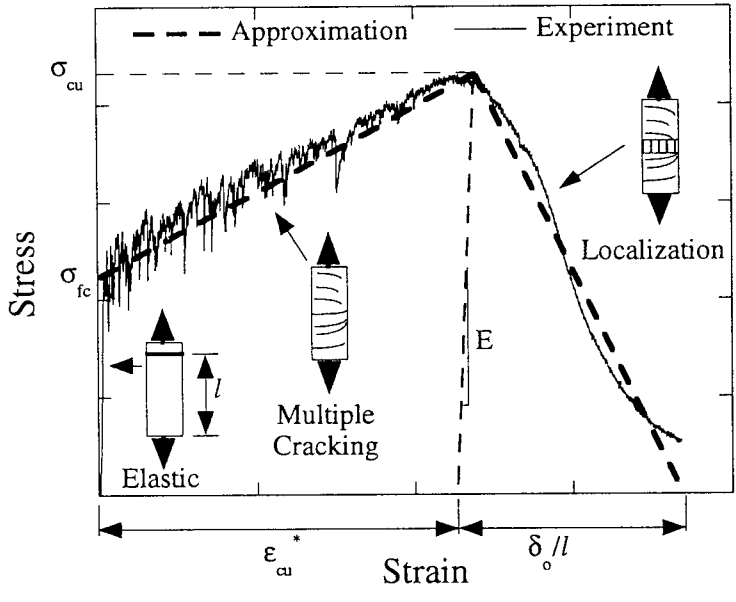

Figure 30. Experimental [62] and approximated uniaxial stress-strain curve for 2% Polyethylene HPFRCC (l = 207 mm, E = 22 GPa, σ_{fc} = 2.2 MPa, σ_{cu} = 4.32 MPa, ε_{cu}^* = 5.78 %, δ_o = 6.62 mm, h = $[\sigma_{cu}-\sigma_{fc}]/\varepsilon_{cu}^*$, s = σ_{cu}/δ_o).

Fig.31 shows the analytical and experimental load displacement curves for a DCB specimen. As indicated, the model is able to reproduce the significant pre-peak

nonlinear behavior, the displacement at peak, and the post-peak branch. However, the model predicts higher load at peak. A possible reason for this could be that the model response reflects the ideal case of material homogeneity.

The model simulation indicated that prior to the bend-over point, both multiple and localized cracks concentrate near the original notch tip. However, during the hardening portion of the P-δ curve, multiple cracks spread rapidly around the notch tip while the localized crack propagates slowly. The distribution of cracking strain and evolution of the localized crack at the peak load is shown in Fig.32. As indicated in Fig.32(a), the multiple cracking zone has an onion like shape and extends almost to the specimen boundaries. This observation is consistent with the experimental results as reported by Li and Hashida [60].

As a further step Kabele and Horii [61] attempted to reproduce the experimental results of Maalej et al. [62] on the effect of fiber volume fraction on the fracture energy of strain hardening polyethylene fiber reinforced cement paste. The fiber volume fractions considered in the analysis were 0.8%, 1%, 2%, and 3%. the Material parameters for the model were determined from the respective uniaxial tensile stress-strain curves. Fig.33 shows a comparison between the model results and the experimental results. We can see that the model can predict the general trend that with increasing fiber volume fraction, the fracture energy initially increases and then becomes saturated. However, the model predicts higher magnitudes of total fracture energy which can be related to the overpredicted peak load of the P-δ curve.

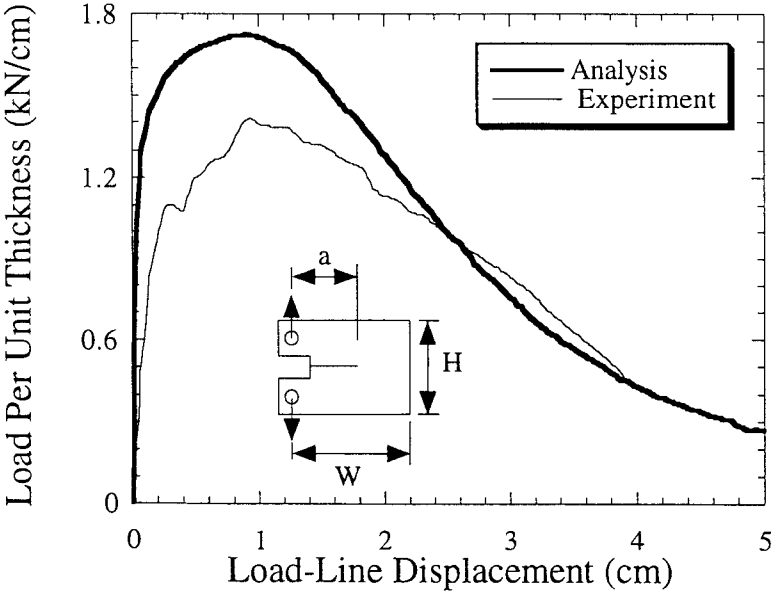

Figure 31. Experimental [60] and Predicted Load-Displacement Curves for DCB specimen (H = 30 cm, W = 31 cm, a = 14.8 cm).

5.5 Conclusions

Significant enhancement in fracture toughness can be achieved with the use of fibers. In FRCC, toughening is attained by frictional pull-out of fibers bridging a matrix crack. The σ–δ curve provides a means of calculating the composite fracture toughness due to this effect. This section demonstrates that when the influence of fiber rupture is taken into account, the micromechanical model predicts an optimal composite toughness associated with specific combinations of fiber, matrix and interface parameters. Orders of magnitude toughness improvement has been observed and predicted based on the fiber friction pull-out mechanism. Toughness improvement can be even higher in HPFRCC in which damage tolerance is greatly enhanced by the blunting effect of multiple cracking. Damage evolution surrounding a notch tip can be modelled based on the uniaxial tensile pseudo strain hardening response.

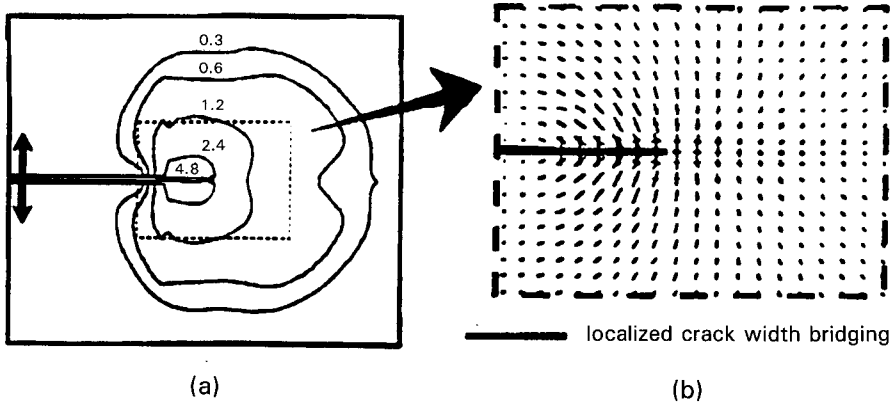

Figure 32. Distribution of Cracking Strain and Evolution of Localized Crack at Peak Load (a) Contour Lines of Maximum Principle Cracking Strain (%); (b) Principle Cracking Strains and Localized Crack Near the Original Notch Tip [61].

6 ELASTIC MODULUS

6.1 Introduction

The elastic response of fiber reinforced cement based composites was modeled by Alwan and Naaman [63] and Alwan [20] using two different approaches. The first approach, based on composite mechanics principles, yielded a mathematical model that predicts the modulus of elasticity of brittle-matrix composites reinforced with ductile discontinuous fibers [63]. The second approach, however, based on energy principles and the homogenization theory, lead to a numerical scheme that is built on a finite element procedure and that predicts the elastic constants of any homogenized fiber reinforced composite [20]. In what follows, a brief summary is introduced on each approach and the resulting model.

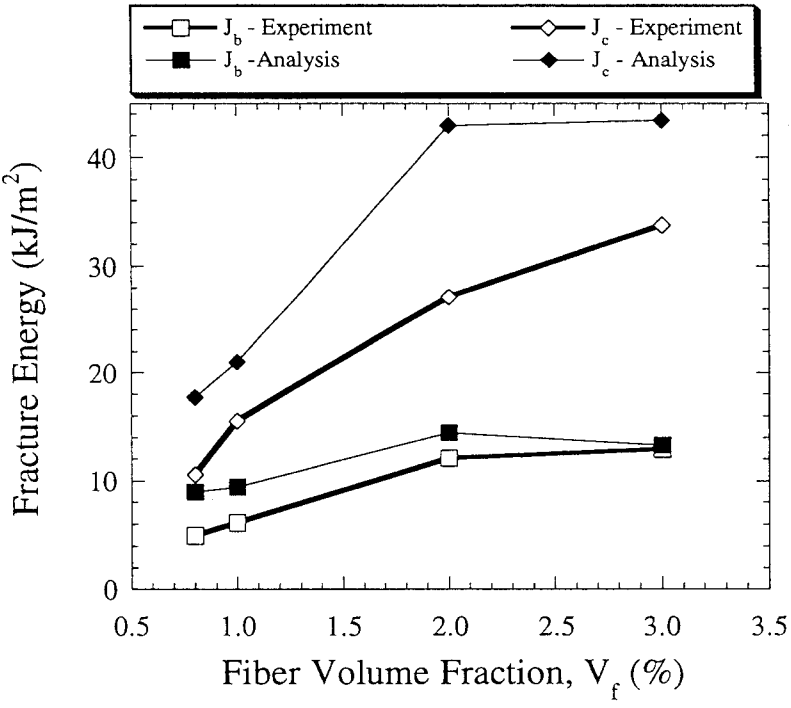

Figure 33. Experimental [62] and Predicted Variation of Fracture Energy as Function of Fiber Volume Fraction.

6.2 Pseudo Three Phase Model

Generally, the elastic modulus of a two-phase composite is predicted from the mechanical properties and proportions of the two components. Here a new approach is introduced in which the interfacial layer surrounding the fiber, viewed as a third phase with zero volume, is modeled as an imperfect bond with mechanical properties similar to or different from the surrounding matrix (Fig. 34). Based on this assumption, new upper (Eqn. 45), and lower bound (Eqn. 46) solutions for the elastic modulus of aligned short fiber composites are analytically derived assuming either a uniform applied strain or a uniform applied stress.

$$E_{c-//_{\text{uniform strain}}} = V_f E_f \left[1 - \frac{\tanh(\lambda L)}{\lambda L}\right] + V_m E_m \tag{45}$$

$$E_{c-//_{\text{uniform stress}}} = \frac{Q E_m}{\left[(Q-1) + \frac{\tanh(\lambda L)}{\lambda L}\right]} \tag{46}$$

Where, L = half fiber length.

$Q = 1 + \frac{E_m A_m}{E_f A_f}$

and $\lambda = \sqrt{\frac{2\pi r_f \kappa}{E_m A_m}\left(1 + \frac{E_m A_m}{E_f A_f}\right)}$

in which r_f = fiber radius,

and κ = interfacial bond modulus.

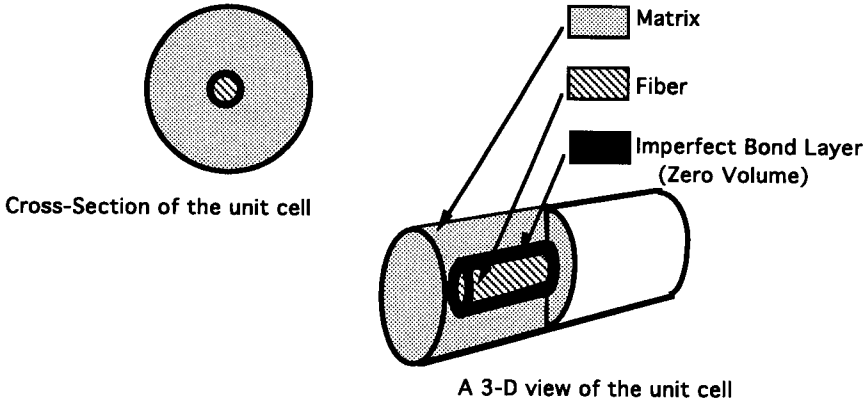

Figure 34. Typical unit cell illustrating the Pseudo-Three-Phase model [63].

The two solutions are then combined linearly (Eqn. 47) to achieve an average modulus of aligned short fiber composite.

$$E_{c\text{-}//_{average}} = \alpha E_{c\text{-}//_{uniform\ stress}} + (1-\alpha) E_{c\text{-}//_{uniform\ strain}} \qquad (47)$$

The usual lower bound solution for the modulus of elasticity of a fiber composite with the fiber normal to the axis of loading is then modified to account for matrix porosity as affected by the presence of fibers (Eqn. 48).

$$E_{c\text{-}\perp_{modified}} = \frac{\left(\frac{1-p}{1-p_o}\right)^3 E_m E_f}{E_f V_m + \left(\frac{1-p}{1-p_o}\right)^3 E_m V_f} \qquad (48)$$

where, p = porosity of matrix with presence of fibers,

and p_o = porosity of matrix with no fibers.

It is finally suggested that the elastic modulus of random short fiber composites (Eqn. 49) be taken as a linear average of the values obtained for the aligned (Eqn.47) and normal (Eqn. 48) fiber values.

$$E_c = \mu E_{c\text{-}//_{average}} + (1-\mu)E_{c\text{-}\perp_{modified}} \quad (49)$$

Comparing the model output with experimental results [57, 58] lead to averaging coefficients of 0.5 in Eqns. (47) and (49), (Fig. 35). This is acceptable because the aligned fiber solution is basically an averaged solution of an upper and a lower bound solution.

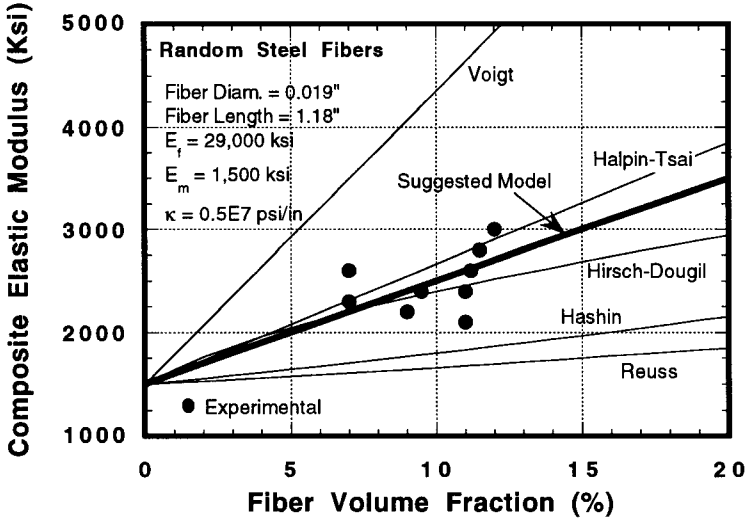

Figure 35 . Comparison of model with experimentally measured data [20].

6.3 Homogenization Based Model

The homogenization theory covers the relations between the microscopic and macroscopic scales through which a heterogeneous material is replaced by an "equivalent" homogeneous one. In the homogenization method, it is usually assumed that a composite is locally formed by the spatial repetition of a micro structure or "microscopic" cells which are small enough when compared to the overall macroscopic dimensions. The composite homogenized elastic constants "L_{mnpq}" are then formulated based on the characteristic response of the unit cell,

$$L_{mnpq} = \frac{1}{|Y|}\int_Y \{ L_{ijkl}(y) \overset{mn}{\chi}_{i,j} \overset{pq}{\chi}_{k,l} \} \, dy \quad (50)$$

where, $L_{ijkl}^{mn\ pq}(y)$ = Elastic constants of constituents as a function of space.

$\chi_{i,j}\chi_{k,l}$ = characteristic deformations due to unit deformations in the **mn** and **pq** directions respectively.

Y = volume of the unit cell.

Such response can be predicted either analytically or numerically, depending on the complexity of the unit cell geometry. Examples on numerical approaches in Homogenization include the implementation of finite element based procedures with homogenization theory [66, 67, 68].

The implementation of the finite element method in computing the homogenized elastic constants of composites can be presented in two steps. First, by examining (Eqn. 50), it can be concluded that the characteristic deformations in the unit cell are to be evaluated over the whole volume of the unit cell. The finite element method allows for the evaluation of the displacement field at discritized nodes in the unit cell as the unit cell is subjected to different boundary conditions. Second, by assembling the global unconstrained stiffness matrix of the modeled unit cell, one would have defined discretely the term related to L_{ijkl} in (Eqn. 50). Therefore, by discretizing the unit cell into smaller elements, and defining the material properties for each discritized element in the unit cell, (Eqn. 50) can be written in the following numerical form

$$L_{mnpq} = \frac{1}{\sum_{i=1}^{n} V^e_i} \overset{mn}{[U]}^T [K] \overset{pq}{[U]} \tag{51}$$

where, $\underset{pq}{[K]}$ = unconstrained stiffness matrix of the unit cell.

$\underset{pq}{[U]}$ = nodal displacement vector due to a unit strain deformation in the p-q direction.

$\overset{mn}{[U]}$ = nodal displacement vector due to a unit strain deformation in the m-n direction.

V^e_i = volume of a discretized element of the base unit cell.

when values of the composite modulus obtained from different unit cells are compared in (Fig. 36), the difference is significant even at low fiber volume fractions. The reason for this difference is that one type of unit cells is symmetrical in the longitudinal and transverse direction (solid dots), while the other type is not. All the fibers in the latter type are aligned in the longitudinal direction, therefore, the homogenized composite is stiffer in that direction than an equivalent composite with only 50% of its fibers aligned in that direction. And while both types of unit cells account for fiber interaction, the first type of unit cell models a quasi-isotropic composite, while the second type models an orthotropic composite.

Since the homogenization-numerical procedure provides the values of the elastic constants of the unit cell. The effective modulus of the fiber composite in any orientation angle for the load application can be easily derived from the computed elastic constants. Thus one can study the effect of fiber orientation on the elastic modulus for various unit cells. Two types of unit cells were used in this comparison. Type [1] unit cells of the quasi-isotropic composite, and type [3] unit cells of the aligned case with fiber interaction. Figs. 37 and 38 are non-dimensional plots of the composite elastic modulus. The plots show the variation of the elastic modulus as a function of the orientation angle θ. θ is the angle between the major axis of fiber alignment and the direction of load application. It may be noted in (Fig. 37) that for the cement based composite system chosen, E_x does not monotonically decrease from E_L at $\theta = 0^\circ$ to E_T at $\theta=90^\circ$. E_x is less than both E_L and E_T for values of θ between 30° and 70°. The

curves shown can be changed considerably by relatively small variations in the properties of the fiber matrix combination. It should be observed from these curves that the extreme values of material properties do not necessarily occur in principal material directions, which is actually the case for E_x, in the cement based composite system.

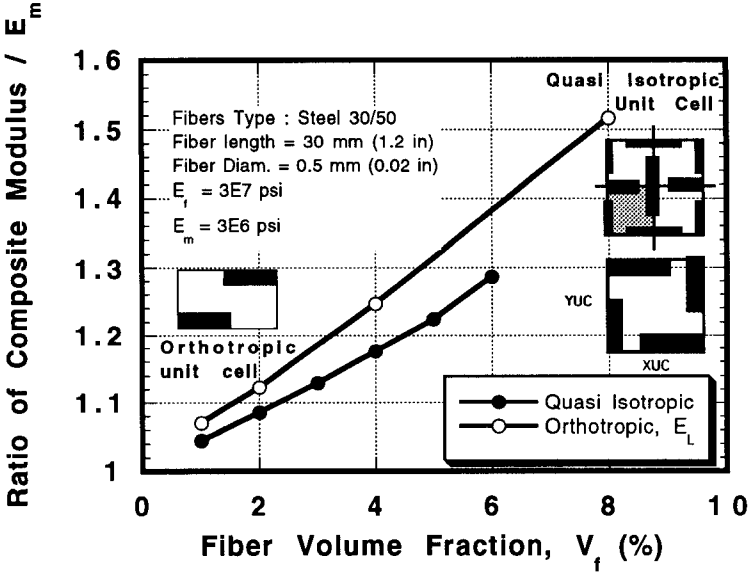

Figure 36 . Comparison between types of unit cells [30/50 steel fibers] [20].

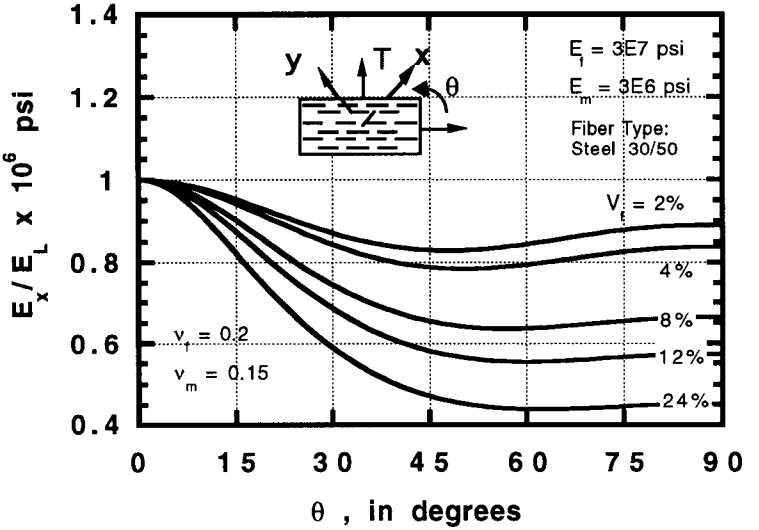

Figure 37 . Variation in the elastic modulus of an aligned short fiber cement composite [20].

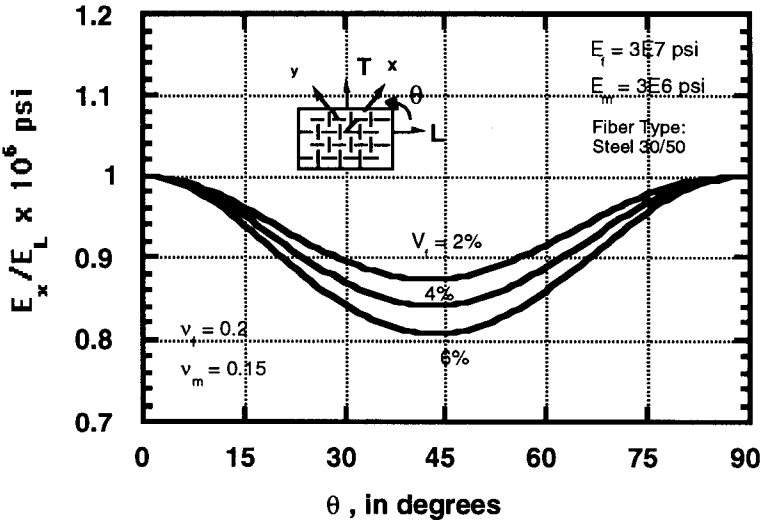

Figure 38 . Variation in the elastic modulus of a balanced short fiber cement composite [20].

Another important factor that affects the composite elastic modulus is the porosity or void content of the matrix. This effect is very critical in cement based composites due to the nature of processing the composite material. (Fig. 39) shows a non-dimensional plot of the composite longitudinal and transverse modulus as a function of the void content by volume. Both moduli decrease at a constant rate and with the same slope as the void content increases. Therefore, the homogenization-numerical procedure has shown flexibility and versatility in the computation of the elastic modulus of composites. It allows for including the effect of void content in the matrix as it allows for the study of other effects such as fiber orientation, fiber packing, and size effect of unit cell.

Finally, the composite elastic modulus was computed by the homogenization model for three different packing orders or proportionality constants of 20, 30, and 50 respectively. The proportionality constant is defined as the ratio of the relative edges of a unit cell. The results are shown in Fig. 40, along with the prediction model from the pseudo-three-phase model. Results obtained by the homogenization model are in good agreement with experimentally measured data. Moreover, the homogenization model shows the effect of the packing order, translated in the proportionality constant, on changing the mechanical properties of composites with similar fiber contents. Thus, providing an analytical tool that can be used in optimizing the elastic response of composites in general by controlling the packing order of the constituents.

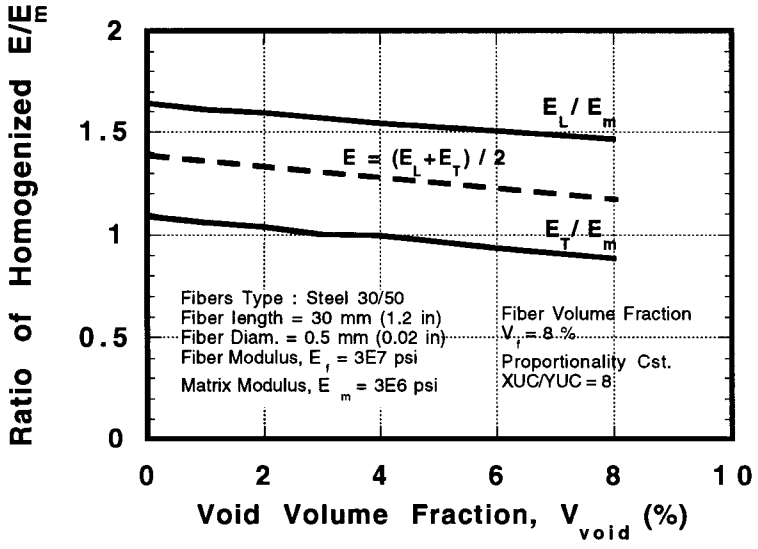

Figure 39 . Effect of void content on the elastic modulus of a random short fiber composite [20].

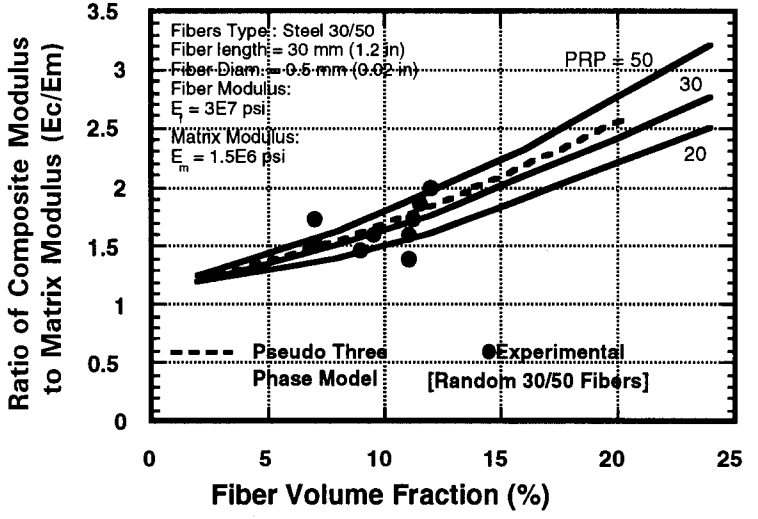

Figure 40 . Comparison of homogenization model with pseudo-three-phase model and experimentally measured data [20].

6.4 Conclusions

Composite modulus can be modelled in terms of fiber parameters. It has been observed that a porous transition zone exists around fibers in cementitious composites (see e.g. Chapter 5). As discussed in Section 3, microdefects can also be introduced into the matrix in the presence of fibers. The present model takes these features into account via a third phase of possibly lower stiffness and via porosity of zero stiffness. This analytic model and a homogenization model more suitable for computation FEM analysis, is shown to predict composite modulus as a function of fiber volume fraction for a HPFRCC well.

7 DISCUSSIONS AND CONCLUSIONS

Over the last decade, micromechanical models have gradually increased in sophistication. The most important advancements may be the enhanced ability to deal with the more complicated short random distribution of fibers more realistic of HPFRCC, as opposed to the simpler continuous aligned fiber arrangement. Additional realism deals with the possibility of fiber rupture, and inclined fiber mechanical interactions with the cementitious matrix. Further, earlier micromechanical models often confined to simulate elastic behavior, are giving way to the modern micromechanical models which addresses important non-linear post-cracking behavior. These behaviors are particularly important in HPFRCC in which fiber efficiencies are often best activated after matrix cracking. At this stage, the classical composite model in which strain compatibility between fiber and matrix is assumed can no longer suffice.

The various micromechanical models collected in this chapter suggest that it is possible to relate composite mechanical properties to micromechanical parameters associated with fiber, cementitious matrix, and interface. That is,

$$\text{Mechanical property} = \text{fcn (fiber, matrix, and interface)} \tag{52}$$

with fiber parameters including fiber length, diameter, modulus and strength, matrix parameters including the matrix modulus, toughness, porosity, flaw size and density/distribution, interface parameters including bond strength and modulus, and snubbing coefficient. These parameters, over ten of them, play different roles and importance to different properties. For example, matrix toughness plays no role in the composite Young's modulus, but is critical to the first crack strength and tensile strain-hardening behavior (and hence the ultimate tensile strain capacity). Other parameters, like the fiber diameter, seems to play important roles in many composite properties. The micromechanical models clarify the governing constituents for each composite property.

The magnitude of improvement derived from fiber reinforcement varies significantly for different composite properties. Table 2 summarizes the % improvement observed in the HPFRCCs discussed in this chapter. Naturally, these values change with different fiber types, volume fraction and other fiber parameters, and also depend on details of processing routes. Even so, it can be observed that fibers can be extremely effective in providing orders of magnitude improvement in composite ductility as measured by tensile strain capacity, and in composite fracture toughness. Moderate improvements can be achieved in composite tensile, compressive or flexural strengths, typically on the order of several times the corresponding matrix strength, but seldom exceeding an order of magnitude. Composite properties such as elastic modulus cannot be improved

by much more than a factor of two. The micromechanical models highlight the reasoning behind these magnitude changes.

In reviewing the various composite properties discussed in this chapter, the micromechanical models reveal a common feature underpinning all (except the elastic modulus) composite properties. This common feature, a more fundamental composite property, is the σ–δ relation. This is not surprising since properties governed by the propagation of cracks can be expected to be influenced by the fiber bridging effect across matrix cracks. The fiber bridging effect is best described by the σ–δ relation, which represents the spring-like 'cohesive' force resisting crack opening. Latest development in σ–δ modeling can be found in [69, 70].

For HPFRCC best characterized by the pseudo strain-hardening response in tension (Chapter 1), the rising branch of the σ–δ relation is more important than the descending branch. This feature is amply brought out in the discussion in this chapter in relation to the condition for pseudo strain-hardening (section 2.3). This rising branch is insignificant and is usually ignored in ordinary FRC.

There is a general trend in recent years in increasing use of microfibers with small fiber diameter in HPFRCC. Because of the small diameter close to or even smaller than the cement grain size, the interfacial bond strength is usually enhanced due to elimination of the weak transition zone (Chapter 5). Reduction in fiber diameter and increase in bond strength leads to improvements in the fiber bridging effectiveness via the σ–δ relation, according to micromechanical models (eqn. 7). Thus, it is not surprising that microfibers can lead to better mechanical performance, if it is not limited by workability problem in the mixing process. As a general rule, smaller fiber diameter usually associates with higher fiber strength (due to molecular alignment in polymer fibers, work-hardening in steel fiber drawing, microflaw elimination in carbon fibers).

It should be clear by now that micromechanical models can provide good physical understanding as well as good basis for microstructure tailoring of composite properties. This is best demonstrated by the pseudo strain-hardening properties. Micromechanics quantifies the critical combination of fiber, matrix and interface properties needed for achieving pseudo strain-hardening.

While the micromechanical models have been shown to predict various important mechanical properties of HPFRCC well, there are still plenty of shortcomings in the present generation of these models. Some of these are pointed out below:

a) Some micromechanical parameters can become inter-dependent, creating a more complex situation for model description. For example, some experiments have indicated that fiber/matrix interface bond strength can deteriorate with fiber content. The rate of deterioration may depend on fiber type and processing details. Another example is illustrated by the micromechanical model described in this chapter for compressive strength. It suggests that matrix defects can be introduced by fibers.
b) Some micromechanical parameters, although physically reasonable, are none-the-less difficult to quantitatively measured. These include pre-existing microcrack size and population, or flaw density. Also measurement of isolated parameters through model composite such as bond strength measurement in a single fiber pull-out test, may not represent the same parameter in a true composite.
c) Some micromechanisms, while reasonably assumed, are not yet directly verified, and may be dependent on the particular matrix, fiber or even processing conditions. In

other situations, certain micromechanisms are observed, but is found to be too complex to implement in a mathematically tractable micromechanical model.

Table 2. HPFRCC properties improvement over plain matrix.

HPFRCC Properties	Improve -ment (%)	Example fiber system	Reference
Tensile first crack strength	10 to 40	2% PE fiber	[4]
	100	4% PVA fiber	[72]
	80	3% Carbon fiber	[73]
Tensile ultimate strength	20 to 200	2% PE fiber	[4]
	500	12% Steel fiber	[74]
	400	12% Steel fiber	[75]
Tensile first crack strain	40	2% PE fiber	[71]
	60	3% Carbon fiber	[73]
Tensile ultimate strain	20000	2% PE fiber	[4]
	2900	12% Steel fiber	[74]
	7900	4% PVA fiber	[72]
	10000	7% PP fiber	[76]
	1750	6% Steel fiber	[77]
Compressive modulus	10 to 50	12% Steel fiber	[74]
Compressive strength	50	2% PE fiber	[16]
	100	1% Aramid fiber	[29]
	150 to 300	12% Steel fiber	[78]
Compressive strain	40 to 100	2% PE fiber	[16] [71]
	300	12% Steel fiber	[78]
Fracture toughness	150000	3% PE fiber	[62]
	600000*	12% Steel fiber	[78]
	170000*	6% Steel fiber	[79]
Flexural strength	500	2% PE fiber	[49]
	150 to 950	14% Steel fiber	[78]
	40 to 160	5 to 20% Steel fiber	[34]
	2000	8% Carbon+cont mesh	[23]
	350	6% Steel fiber	[79]

*From area under load deflection curves.

The shortcomings of the present generation of micromechanical models point to challenges for the research community. In addition, there are urgent needs for investigations in the following areas:

a) Composite microstructure tailoring: More concerted effort at bringing micromechanical models to bear on composite property design via microstructure tailoring. With further micromechanical model refinements, composite microstructure tailoring represents an immense opportunity for creating greatly enhanced properties in the next generation HPFRCC.
b) Integrated studies of composite properties using a consistent set of micromechanical parameters. This is in contrast to current investigations where only one property is investigated at one time.
c) Expand the coverage of mechanical properties to include more complex loading histories, such as fatigue properties, or mechanical responses under multi-axial loading

conditions, and to include time-dependency of composite property via time-dependency of certain micromechanical parameters.

d) Linking microstructure via composite properties to structural performance. Ultimately, HPFRCC are desired for their ability to enhance the performance of structural elements or systems. It would be most desirable if HPFRCC can be designed according to specific structural performance or functional needs. Micromechanical models can serve to achieve this objective.

8 REFERENCES

[1] Li, V.C. & Leung, C.K.Y., Theory of Steady State and Multiple Cracking of Random Discontinuous Fiber Reinforced Brittle Matrix Composites. ASCE J. Eng. Mech., 118(11), 1992, 2246-2264.

[2] Leung, C.K.Y., Design Criteria for Pseudo-ductile Fiber Reinforced Composites. in press, ASCE J. Eng. Mech, 1995.

[3] Li, V.C., and Wu, H.C., Conditions for Pseudo Strain-Hardening in Fiber Reinforced Brittle Matrix Composites, Appl. Mech. Rev., Vol. 45, No. 8, 1992, 390-398.

[4] Li, V.C., Wu, H.C., and Chan, Y.W., Effect of Plasma Treatment of Polyethylene Fibers on Interface and Cementitious Composite Properties, accepted by J. of Amer. Cer. Soc., 1994.

[5] Stang, H., Mobasher, B. and Shah, S.P., Quantitative Damage Characterization in Polypropylene-Fiber-Reinforced Concrete, Cem. & Concr. Res., 20, 1990, 540-558.

[6] Mobasher, B., Castro-Montero, A. and Shah, S.P., A Study of Fracture in Fiber-Reinforced Cement-Based Composites Using Laser Holographic Interferometry. Exp. Mech., 30, 1990, 286-294.

[7] Yang, C.C., Mura, T. and Shah, S.P. , Micromechanical Theory and Uniaxial Tensile Tests of Fiber-Reinforced Cement Composites. J. Mat. Res., 6(11), 1991.

[8] Marshall, D.B., Cox, B.N. & Evans, A.G., The Mechanics of Matrix Cracking in Brittle-Matrix Fiber Composites. Acta Metall., 33(11), 1985, 2013-2021.

[9] Leung, C.K.Y. and Li, V.C., First Cracking Strength of Short Fiber Reinforced Ceramics. Ceram. Eng. Sci. Proc., 10(9-10), 1989, 1164-1178.

[10] Marshll, D.B. and Cox, B.N., A J-Integal Method for Calculating Steady-State Matrix Cracking Stresses in Composites. Mechanics of Materials, 7, 1988, 127-133.

[11] Li, V.C., From Micromechanics to Structural Engineering - The Design of Cementitious Composites for Civil Engineering Applications. Structural Engineering/Earthquake Engineering, 10(2), 1993, 37-48.

[12] Li, V.C., Postcrack Scaling Relations for Fiber Reinforced Cementitious Composites, J. of Materials in Civil Engineering, Vol. 4, No. 1, 1992, 41-57.

[13] Li, V.C., Wang, Y., and Backer, S., Effect of Inclining Angle, Bundling, and Surface Treatment on Synthetic Fiber Pull-Out from a Cement Matrix, J. Composites, Vol. 21, No. 2, 1990, 132-140.

[14] Maalej, M., Li, V.C., and Hashida, T., Effect of Fiber Rupture On Tensile Properties of Short Fiber Composites, Accepted for Publication in the ASCE Journal of Engineering Mechanics, 1994.

[15] Li, V.C., and K.H. Obla, Effect of Fiber Length Variation on Tensile Properties of Carbon Fiber Cement Composites, *Int'l J. of Composites Engineering*, Vol. 4, No. 9, 1994, 947 - 964.

[16] Li, V.C. , Mishra, D.K., & Wu, H.C., Matrix Design for Pseudo Strain-Hardening Fiber Reinforced Cementitious Composites. Accepted for publication in the RILEM J. of Materials and Structures, 1994.

[17] Krenchel, H., see chapter 6, 1995.
[18] Aveston, J., Cooper, G.A., and Kelly, A., Single and Multiple Fracture. in The Properties of Fiber Composites, IPC Science and Technology Press, Guildford, U.K., 1971, 15-26.
[19] Wu, H.C., and Li, V.C., Stochastic Process of Multiple Cracking in Discontinuous Random Fiber Reinforced Brittle Matrix Composites. Inter. J. Damage Mechanics, 4(1), 1995, 83-102.
[20] Alwan, J. M., Modeling of The Mechanical Behavior of Fiber Reinforced Cement Based Composites Under Tensile Loads, *Ph. D. Thesis*, Department of Civil and Environmental Engineering, University of Michigan, Ann Arbor, August 1994.
[21] Ohno, S., and Hannant, D., Modeling the Stress-Strain Response of Continuous Fiber Reinforced Cement Composites, ACI Materials J., 91-3, 1994, 306-312.
[22] Al-Shnnaq, M.J. ,Tensile Behavior of Fiber Reinforced DSP, Ph.D Thesis, Department of Civil Engineering, University of Michigan, 1995.
[23] Brincker, R., contribution to this chapter, 1995.
[24] Stang, H. and Aarre, T. , Evaluation of Crack Width in FRC with Conventional Reinforcement, Cem. & Concr. Composites, 14, 1992.
[25] Hayashi, R., Yamada, K., Inaba, S., and Tsubouchi, S., Tensile Properties of Carbon Fiber Mesh Reinforced Mortar with Various Weavings, proc. of the Japan Concrete Institute, 12-1, 1043-1048, 1990 (in Japanese).
[26] Mihashi, H., Contribution to this chapter, 1995.
[27] Shah, S. P., and Rangan, B. V., Fiber Reinforced Concrete Properties, *J. of ACI, Proceedings*, Vol. 68, No. 2, 1971, 126-135.
[28] Fannela, D. A., and Naaman, A. E., Stress-Strain Properties of Fiber Reinforced Concrete in Compression, *J. of ACI, Proceedings*, Vol. 82, No. 4, 1983, 475-483.
[29] Akihama, S., Nakagawa, H., Takada, T. and Yamaguchi, M., Experimental study on aramid fiber reinforced cement composites "AFRC" mechanical properties of AFRC with short fibers. In RILEM Symposium on Developments in Fiber Reinforced Cement and Concrete, FRC86, Vol. 1, Swamy, R.N, Wagstaffe, R.L. and Oakley, D.R. (ed.), Paper 2.5, 1986.
[30] Ward, R., Yamanobe, K., Li, V.C., and Backer, S., Fracture Resistance of Acrylic Fiber Reinforced Mortar in Shear and Flexure, in *Fracture Mechanics: Application to Concrete*, Eds. V. Li and Z. Bazant, ACI SP-118, 1989, 17-68.
[31] Zhu, B.Y., Behavior of Concrete with Synthetic Organic Fibers, in *Darmstadt Concrete*, Vol. 5, 1990, 249-255.
[32] Tjiptbroto, P., Tensile Strain Hardening of High Performance Fiber Reinforced Cement Based Composites. *Ph.D. Thesis*. Department of Civil Engineering, University of Michigan, 1991.
[33] Naaman, A. Otter, D. and Najim, H., Elastic Modulus of SIFCON in Tension and Compression. ACI *Materials Journal*, Vol. 88, No. 6, Nov.-Dec., 1991, 603-612.
[34] Rossi, P., T. Sedran, S. Renwez, and A. Belloc, Ultra-High-Strength Steel Fibre Reinforced Concretes: Mix Design and Mechanical Characterization, in Fiber Reinforced Concrete - Modern Developments, N. Banthia, S. Mindess, UBC Press, Canada, 1995, 181-186.
[35] Li, V. C., A Simplified Micromechanical Model of Compressive Strength of Fiber Reinforced Cementitious Composites, *J. of Cement and Concrete Composites*, 14, 1992, 131-141.
[36] Li, V.C. and Mishra, D.K., Micromechanics of Fiber Effect on the Uniaxial Compressive Strength of Cementitious Composites. In *RILEM 4th Inter. Symp. on Fiber Reinforced Concrete,* R.N. Swamy (ed.), E&FNSpon, 1992.

[37] Horii, H. and Nemat-Nasser, S., Brittle Failure in Compression: Splitting, Faulting, and Brittle-Ductile Transition. *Phil. Trans. Royal Soc. London*, 319, 1986, 337-374.
[38] Ashby, M.F. and Hallam, S.D., The Failure of Brittle Solids Containing Small Cracks under Compressive Stress States. *Acta Metall.* 34 No. 3, 1986, 497-510.
[39] Kemeny, J. M., and Cook, N.G.W., Micromechanics of Deformation in Rocks. In *Toughening Mechanisms in Quasi-Brittle Materials*, S.P. Shah (ed.), Kluwer Academic Publishers, 1991, 155-188.
[40] Glavind, M., Evaluation of Compressive Behavior of Fiber Reinforced High Strength Concrete, Ph.D. Thesis, Technical University of Denmark, 1992.
[41] Yin, W. S., Su, C. M., Mansur, M.A., and Hsu, T.T.C., Fiber Reinforced Concrete Under Biaxial Compression, *Engineering Fracture Mechanics*, Vol. 35, No. 1/2/3, 1990, 261-268.
[42] Hillerborg, A., Modéer, M., and Petersson, P.E., Analysis of Crack Formation and Crack Growth in Concrete by Means of Fracture Mechanics and Finite Elements. *Cement and Concrete Research*, 6, 1976, 773-782.
[43] Zhu, Y., The Flexural Strength Function for Concrete Beams Without Initial Cracks, Proceedings of the 8th European Congress of Fracture: Fracture Behavior and design of Materials and Structures, Volume II, D. Firrao, ed., Chameleon Press LTD., London, 1990, 599-604.
[44] Ward, R. and Li, V.C., Dependence of Flexural Behavior of Fiber Reinforced Mortar on Material Fracture Resistance and Beam Size, *J. Materials*, American Concrete Institute, 87(6), 1990, 627-637.
[45] Maalej, M., and Li, V. C., Flexural Strength of Fiber Cementitious Composites, *ASCE J. of Materials in Civil Engineering*, 6(3), 1994, 390-406.
[46] Katz, A., and Bentur, A., Mechanisms and Processes Leading to Changes in Time in the Properties of Carbon Fiber Reinforced Cement, Advn. Cem. Bas. Mat., accepted for publication, 1995.
[47] Torrent, R.J. and Brooks, J.J., Application of the Highly Stressed Volume Approach to Correlated Results from Different Tensile Tests of Concrete, Magazine of Concrete Research (London), Vol. 37, No. 132, 1985, 175-184.
[48] Johnston, D., Steel Fiber Reinforced and Plain Concrete: Factors Influencing Flexural Strength Measurement, ACI Journal, Proceedings, 79(2), 1982, 131-138.
[49] Maalej, M., and Li, V. C., Flexural/Tensile-Strength Ratio in Engineered Cementitious Composites, *ASCE J. of Materials in Civil Engineering*, 6(4), 1994, 513-528.
[50] Li, V.C., Wu, H.C., Maalej, M., Mishra, D.K., and Hashida T., Tensile Behavior of Engineered Cementitious Composites with Discontinuous Random Steel Fibers, Accepted for publication in J. Amer. Ceramic Soc., 1994.
[51] Cottrell, A. H., Strong Solids, *Proc.Roy. Soc.*, A282, 1964, 2-9.
[52] Cooper, G. A. and Kelly, A., The Contribution to the Work of Fracture of a Composite Material of Pull-Out of Fibers, in *Mechanics of Composite Materials*, eds. F. W. Wendt, H. Liebowitz, and N. Perrone, Pergamon Press, Oxford, 1970, 653-661.
[53] Kelly, A. and Macmillan, N. H., *Strong Solids*, Clarendon Press, Oxford, 1986.
[54] Visalvanich, K., and Naaman, A.E., Fracture Model for Fiber Reinforced Concrete, ACI Journal, Vol. 80, No. 2, 1983, 128-138.
[55] Li, V.C., Wang, Y., and Backer, S., A Micromechanical Model of Tension Softening and Bridging Toughening of Short Random Fiber Reinforced Brittle Matrix Composites, J. Mech. Phys. Solids, Vol. 39, No. 5, 1991, 607-625.
[56] Visalvanich, K., and Naaman, A.E., Fracture Modeling of Fiber Reinforced Cementitious Composites, Program Report for NSF Grant ENG 77-23534,

Department of materials Engineering, University of Illinois at Chicago Circle, 1982.

[57] Wang, Y., Li, V.C., and Backer, S, Tensile Properties of Synthetic Fiber Reinforced Mortar, *J. Cement and Concrete Composites*, Vol. 12, No. 1, 1990, 29-40.

[58] Wang, Y., Li, V.C., and Backer, S, Tensile Failure Mechanisms in Synthetic Fiber-Reinforced Mortar, *Journal of Materials Science*, Vol. 26, 1991, 6565-6575.

[59] Li, V.C., Wu, H.C., and Chan, Y.W., Interfacial Property Tailoring for Pseudo Strain Hardening Cementitious Composites, in Advanced Technology on Design and Fabrication of Composite Materials and Structures, eds. Carpienteri and Sih, 1993.

[60] Li, V.C. and Hashida, T., Ductile Fracture in Cementitious Materials? *Fracture Mechanics of Concrete Structures*, Z. P. Bazant, ed., Elsevier Applied Science, London, 1992, 526-535.

[61] Kabele, P. and Horii, H. Analytical Modeling and Fracture Analysis of Engineered Cementitious Composites, to appear in Proc. of the 5th East Asia-Pacific Conference on Structural Engineering and Construction, Wollongong, NSW, Australia, 25-27 July, 1995.

[62] Maalej, M., Li, V.C., and Hashida, T., Effect of Fiber Volume Fraction on the Off-Crack-Plane Fracture Energy in Strain Hardening Engineered Cementitious Composites, Accepted for Publication in J. Amer. Cer. Soc., 1994.

[63] Alwan, J. M., and Naaman, A. E., New Formulation for Elastic Modulus of Fiber Reinforced, Quasi Brittle Matrices, *ASCE Journal of Engineering Mech.*, Vol. 120, No. 11, Nov., 1994, 2443-2460.

[64] Naaman, A. E., Otter, D., and Najm, H. ,Elastic Modulus of SIFCON in Tension and Compression, *ACI Materials Journal*, Vol. 89, No. 5, 1992, 517-520.

[65] Najm, H., and Naaman, A. E.,Prediction Model For The Elastic Modulus of High Performance Fiber Reinforced Cement Based Composites, *Report No. UMCEE 9217*, Department of Civil and Environmental Engineering, University of Michigan, Ann Arbor, 1992.

[66] Abeyaratne, R., and Triantafyllidis, N. An Investigation of Localization in a porous Elastic Material Using Homogenization Theory , *J. Appl. Mech.*, 51, 1984, 481-486.

[67] Triantafyllidis, N., and Maker, B., On The Comparison Between Microscopic and Macroscopic Instability Mechanisms in a Class of Fiber Reinforced Composites:, *J. Appl. Mech.*, 52, 1985, 794-800.

[68] Guedes, J. M., Nonlinear Computational Models For Composite Materials Using Homogenization, Ph.D. Thesis, Department of Applied Mechanics, University of Michigan, 1990.

[69] Li, V.C., H. Stang, and H. Krenchel, Micromechanics of Crack Bridging in Fiber Reinforced Concrete, J. of Materials and Structures, 26, 486 - 494, 1993.

[70] Stang, H., V.C. Li, and H. Krenchel, Design and Structural Applications of Stress-Crack Width Relations in Fiber Reinforced Concrete, J. of Materials and Structures, 28, 1995, 210-219.

[71] Mishra, D.K., Design of Pseudo Strain-Hardening Cementitious Composites for a Ductile Plastic Hinge, Ph.D. Thesis, The Department of Civil and Environmental Engineering, The University of Michigan, 1995.

[72] Shao, Y., Markunte, S., and Shah, S.P., Extruded Fiber Reinforced Composites, Accepted by Concrete International Magazine, 1994.

[73] Akihama, S., Suenage, T., and Banno, T., Mechanical Properties of Carbon Fiber Reinforced Cement Composite and the Application of Large Domes,

Kajima Institute of Construction Technology, Kajima Corporation, Tokyo, Japan, July, 1984.
[74] Naaman, AE., and Homrich, J.R., Tensile Stress-Strain Properties of SIFCON, ACI Materials J., 86[3], 1989, 244-251.
[75] Tjiptobroto, P. and Hansen, W., Tensile Strain Hardening and Multiple Cracking in High Performance Cement Based Composites Containing Discontinuous Fibers, ACI Materials J., 90[1], 1993, 16-25.
[76] Krenchel, H., and Hansen, S., Durability of Polypropylene Fibers in Concrete, Nordic Concrete Research, No. 6, 143-153, 1987.
[77] Cheyrezy, M.H., see Chapter 2.
[78] Naaman, A.E., SIFCON: Tailored Properties for Structural Performance, in High Performance Fiber Reinforced Cement Composites, eds. H.W. Reinhardt and A.E. Naaman, E&FN Spon, London, 1992, 18-38.
[79] Richard, P., and Cheyrezy, M.H., Reactive Powder Concretes with High Ductility and 200-800 MPa Compressive Strength, in Proc. of Concrete Technology, Past, Present, and Future, ed. P. Kumar Mehta, American Concrete Institute, 1994.
[80] Babut, R., and Brandt, A.M., The Method of Testing and Analyzing of Steel Fiber Reinforced Concrete Elements in Flexure, Proc. RILEM Symp., Testing and Test Methods of Fiber Cement Composites, R.N. Swamy ed., The Construction Press, 1978, 479-486.